



# METIS

Seismic Risk Assessment  
for Nuclear Safety

Research & Innovation Action

NFRP-2019-2020

# **Report on efficient uncertainty quantification and propagation techniques**

## **Deliverable D6.4**

Version N°1

### Authors:

Gerontati Angeliki (NTUA)  
Karaferis Nikolaos (NTUA)  
Vamvatsikos Dimitrios (NTUA)  
Seyed Masoud Nabizadeh (TUK)  
Fathabadi Shadi (TUK)  
Goldschmidt Konstantin (TUK)



## Disclaimer

The content of this deliverable reflects only the author's view. The European Commission is not responsible for any use that may be made of the information it contains.



## Document Information

Grant agreement	945121
Project title	Methods And Tools Innovations For Seismic Risk Assessment
Project acronym	METIS
Project coordinator	Dr. Irmela Zentner, EDF
Project duration	1 <sup>st</sup> September 2020 – 31 <sup>st</sup> May 2025 (57 months)
Related work package	WP 6 – Beyond Design and Fragility Analysis
Related task(s)	Task 6.4 – Report on efficient uncertainty quantification and propagation techniques and implementation in open source software
Lead organisation	NTUA
Contributing partner(s)	NTUA, TUK, IRSN, UL
Due date	31 <sup>th</sup> May 2024
Submission date	15/05/2024
Dissemination level	Public

## History

Version	Submitted by	Reviewed by	Date	Comments
N°1	Angeliki Gerontati, Dimitrios Vamvatsikos	David BOUJITI	15/11/2023	
N°2	Angeliki Gerontati, Dimitrios Vamvatsikos	Shadi Fathabadi	30/04/2024	
N°3	Angeliki Gerontati, Dimitrios Vamvatsikos	Irmela Zentner	27/05/2024	



## Table of Contents

1. Definition of uncertainty quantification and propagation for fragility analysis....	10
1.1. General description.....	10
1.2. Latin Hypercube Sampling.....	11
1.3. Sobol sequence .....	13
1.4. First-Order Second-Moment .....	15
1.5. Comparison of methods .....	16
2. Uncertainty quantification from literature and recommendations .....	18
2.1. Ground Motion .....	18
2.2. Structural damping .....	19
2.3. Structural modelling.....	19
2.4. Structural response phasing .....	20
2.5. Foundation-Structure interaction .....	21
2.6. Earthquake component combination .....	22
2.7. Structural response factor of equipment.....	22
3. Implementation case studies.....	24
3.1. Single degree of freedom system.....	24
3.2. Pump located on NPP reactor building .....	28
4. Conclusion .....	40
5. Acknowledgments .....	40
6. Bibliography .....	40

## List of figures

Figure 1: A progressive LHS design for two uniformly distributed variables is doubled in size by subdividing each stratum to insert new observations: (a) generation 1; (b) generation 2; (c) generation 3; (d) generation 4 (adopted from Vamvatsikos 2014) .....	13
Figure 2: The first eight points of the base 2 Van der Corput sequences (McClarren, 2018). .....	14
Figure 3: Filling a two-dimensional space with 500 random samples.....	16
Figure 4: (a) Comparison of the samples required to achieve the same accuracy (b) comparison of RMSE among different sampling approaches for estimating $\pi$ . ..	17
Figure 5: The target spectra which has been used to generate the simulated signals .....	24



Figure 6: LHS based fragility parameters  $A_m$  (a) and  $\beta$  (b) depending on the number of samples considered. .... 26

Figure 7: Mean squared error of fragility parameter for 10 to 400 samples for (a)  $A_m$  (b)  $\beta$ . .... 27

Figure 8: Fragility curves for (a) LHS, (b) Sobol, (c) Halton, and (d) collectively. .... 28

Figure 9: Original AP1000 reactor design (left) and the corresponding masses-and-sticks model (right) per EPRI (2007). .... 29

Figure 10: Cones for different degrees of freedom (Wolf, 1998). .... 30

Figure 11: Cone model (left) and mass-spring-damper system (right). .... 31

Figure 12: Original model of the service water pump (left) and simplified motor stand model per EPRI (2018) (right). .... 31

Figure 13: Pump motor stand model (left) and hysteretic behavior of the model under static cyclic loading (right). .... 32

Figure 14: Distribution of dispersion for  $S_a$  over a range of periods from 0 to 0.5s. "Period-independent" dispersions for  $AvgS_a(0.1-0.4s)$ ,  $AvgS_a(0.1-0.2s)$  and  $AvgS_a(0.05-0.15s)$  are also indicated with straight lines. .... 37

Figure 15: The maximum relative error of the median and dispersion in IM terms based on CLHS. .... 38

Figure 16: The maximum relative error of the median and dispersion in IM terms based on Sobol sequence. .... 39

Figure 17: The maximum relative error of the median and dispersion in IM terms based on PLHS. .... 39

## List of tables

Table 1: Ground motion variables with their logarithmic standard deviations. .... 18

Table 2: Damping variable with its logarithmic standard deviations. .... 19

Table 3: Modelling variables with their logarithmic standard deviations for structural response. .... 20

Table 4: Modelling variables with their logarithmic standard deviations for equipment response. .... 20

Table 5: Structure response phasing variables with their logarithmic standard deviations. .... 21

Table 6: Foundation-structure interaction phasing variables with their logarithmic standard deviations. .... 22

Table 7: Earthquake component combination variable with its logarithmic standard deviations of structural response. .... 22

D6.4 Report on efficient uncertainty quantification and propagations techniques



Table 8: Earthquake component combination variable with its logarithmic standard deviations of equipment response. .... 22

Table 9: Logarithmic standard deviations of equipment response. .... 23

Table 10: Properties of SDOF ..... 24

Table 11: Stiffness-modification factors for the reactor building and the soil and the corresponding fundamental period of the model per each of 12 LHS realizations. .... 33

Table 12: Number of analyses of the reactor building and the pump and number of records leading to number of IDAs performed..... 34

Table 13: Medians of fragility curves given the IM for the R2R only analysis versus the three uncertainty propagation methods. All values in units of g. .... 35

Table 14: Dispersions of fragility curves given the IM for the R2R only analysis versus the three uncertainty propagation methods. .... 36



## Abbreviations and Acronyms

Acronym	Description
NPP	Nuclear Power Plant
UQ	Uncertainty Quantification
SSC	System, Structure, Component
SSI	Soil Structure Interaction
MCS	Monte Carlo Simulation
LHS	Latin Hypercube Sampling
CLHS	Classic Latin Hypercube Sampling
PLHS	Progressive Latin Hypercube Sampling
FOSM	First-Order Second-Moment
IM	Intensity Measure
SMA	Seismic Margin Assessment
SPRA	Seismic Probabilistic Risk Assessment
HCLPF	High Confidence Low Probability of Failure
RMSE	Root Mean Square Error
GMI	Ground Motion Incoherence
GMRS	Ground Motion Response Spectra
PSHA	Probabilistic Seismic Hazard Analysis
UHRS	Uniform Hazard Response Spectrum
ECC	Earthquake Component Combination
PGA	Peak Ground Acceleration
S <sub>a</sub>	Spectral acceleration
AvgS <sub>a</sub>	Average Spectral acceleration
EDP	Engineering Demand Parameter
CDF	Cumulative Distribution Function



## Summary

The work presented in this report is a part of WP6, which primarily focuses on techniques for efficient uncertainty quantification and propagation, and the subsequent implementation of these techniques in open-source software. The conclusions drawn in this report will be utilized in WP6 to estimate the response of Systems, Structures, and Components (SSCs) of Nuclear Power Plants (NPPs) and to quantify fragility functions. The report provides an overview of the state-of-the-art regarding uncertainty propagation methods when accounting for uncertainties arising from model parameters in structural response assessment. These methods range from computationally expensive, such as Monte Carlo Simulation (MCS) paired with Classic or Progressive Latin Hypercube Sampling (CLHS or PLHS, respectively), Sobol sequences, and Halton Sequences, to generally simpler, often more cost-effective, but typically less accurate methods, such as First-Order Second-Moment techniques (FOSM). The report also highlights the advantages and limitations of these methods and outlines the steps for applying them in the case studies of two simple systems, namely (i) an elastic-hardening single-degree-of-freedom oscillator, and (ii) a service water pump with a moderately pinching force-displacement hysteretic behavior attached to a simplified model of the nuclear power plant's reactor building. Both cases have been set up so that the uncertainties have a non-negligible effect on the fragility curve and should therefore be quantified with accuracy. For the size of the models considered, all MCS-based techniques are found to be more than satisfactory, offering accurate results with low dispersion. Still, among them PLHS is found to be the most efficient technique, combining accurate results with a controllable computational cost, as one does not need to define a priori the number of structural model realizations and the underlying LHS scheme efficiently explores the parameter space. Similar advantages are shared by Sobol and Halton Sequences, but they are not realized for the small parameter spaces explored herein. The report also delves into the applicability of these methods in the context of exploring different scalar ground motion Intensity Measures (IMs). Fragility curves obtained using spectral acceleration at the fundamental period of the component and average spectral acceleration at a range of low periods bracketing the component period showed the lowest overall dispersion, offering evidence in favor of further exploring such IMs for NPP seismic assessments.

## Keywords

fragility assessment, components, uncertainty propagation, material uncertainty, modelling uncertainty, intensity measure



## Introduction

The objective of Deliverable D6.4 “Report on efficient uncertainty quantification and propagation techniques and implementation in open-source software” is to present techniques and detailed information on uncertainty quantification and propagation used to evaluate the fragility of Systems, Structures, and Components (SSCs). Uncertainty quantification (UQ) is the process of assessing and quantifying the uncertainty in the output of a mathematical model or simulation. In the context of nuclear power plants, UQ can be utilized to propagate the uncertainties through the models used to assess the safety and reliability of the plant. Efficient UQ involves the use of techniques that can accurately and efficiently quantify uncertainty while minimizing computational cost. The aim of efficient UQ is to reduce the computational time and resources needed to obtain precise results, making it easier to perform large-scale simulations and model evaluations.

One method of efficient UQ is the use of surrogate models, which are simplified models that approximate the behavior of the original model while requiring less computational cost. Surrogate models can be created using methods such as polynomial chaos expansion, Gaussian process regression, or artificial neural networks. Another approach to efficient UQ is the application of variance reduction techniques, which aim to decrease the variance in the output of a simulation by virtue of near-optimally sampling the input parameters. Techniques such as Monte Carlo simulation and Latin Hypercube sampling can be employed to efficiently explore the parameter space and identify regions of interest. This report focuses on the latter approach to derive the fragility functions.

Within this report, Section 1 provides an overview of uncertainty propagation methods and their critical aspects, focusing on the state-of-the-art in this field. The aim is to present a comprehensive understanding of the current knowledge and advancements in uncertainty propagation techniques. By examining the literature and research findings, this section offers insights into the key principles, challenges, and considerations involved in the application of uncertainty propagation methods. The information presented serves as a foundation for further discussions and analysis in subsequent sections of the report. In Section 2, we provide a review of values for aleatory randomness and epistemic uncertainty provided in literature, codes and other relevant recommendations. Following, in Section 3 we outline the steps for applying simulation-based fragility assessment to two case studies. More specifically, a set of experiments are conducted to evaluate the suitability of uncertainty propagation methods in assessing the fragility of a simple nonlinear single degree of system and then for a service water pump located in the reactor building of a nuclear powerplant. We identify the most efficient method and investigate alternative options as uncertainty-robust intensity measures for the fragility functions. Conclusions and perspectives are given in Section 4.



# 1. Definition of uncertainty quantification and propagation for fragility analysis

## 1.1. General description

Nuclear Power Plants are complex systems involving a wide range of SSCs. The accurate estimation of the seismic demand and capacity of the SSCs is crucial, guaranteeing the secure and dependable design, operation, and maintenance of the powerplant. On the other hand, their seismic performance is heavily influenced by various sources of uncertainty and variability. Uncertainty quantification is a useful tool, which encompasses the quantification and propagation of uncertainties stemming from the inputs, parameters, and models utilized in the performance estimation.

The concept of uncertainty quantification has been effectively incorporated into the Performance-Based Earthquake Engineering (PBEE) framework (Cornell & Krawinkler, 2000; Moehle & Deierlein, 2004; Yang et al., 2009), as proposed by the Pacific Earthquake Engineering Research Center (PEER) to integrate seismic hazard analysis, structural analysis, damage analysis, and loss analysis to provide engineers and stakeholders with the necessary decision-making tools. Several studies, such as those of Lee & Mosalam (2005), Liel et al. (2009), Vamvatsikos & Fragiadakis (2010) as well as the FEMA P-58-1 (2018) guidelines, explicitly address the propagation of uncertainty within the PBEE approach. Seismic hazard analysis involves estimating the probabilities of exceeding given ground motion intensities and it incorporates UQ to account for uncertainties in seismic source, path, and site effects. Structural analysis assesses the response of the structure subject to the given ground motion intensities, with UQ utilized to account for uncertainties in modelling, including the model type and model parameters. Damage analysis evaluates the level and extent of damage to the structure for given levels of structural response, with UQ employed to account for uncertainties in damage models and inspection data. Finally, loss analysis estimates the direct and indirect economic losses arising from damage to the structure, using UQ to account for uncertainties in the loss models and associated input parameters.

For the assessment of an NPP under seismic hazard (e.g., see Huang et al. 2011), Seismic Margin Assessment (SMA) and Seismic Probabilistic Risk Assessment (SPRA) frameworks are used based on NUREG-1407 (Chen et al., 1991). SMA seeks to identify critical components and systems in an NPP and determine the High-Confidence-Low-Probability-of-Failure (HCLPF) capacity of each critical component and plant damage state. SPRA is used to compute the seismic risk of an NPP and to identify the ground-motion intensity level and plant components that have the highest contribution to the risk. SPRA requires the characterization of seismic hazard, the development of fragility data of SSCs, and the estimation of their damage states, while it employs tools such as event trees and fault trees to establish accident sequences that lead to undesirable performance, such as core damage and release of radiation. By integrating hazard and vulnerability results, it determines the annual frequency of said unacceptable performance.

The seismic performance of any SSC is subject to the influence of both aleatory randomness ( $\beta_R$ ) and epistemic uncertainty ( $\beta_U$ ). Aleatory randomness denotes the inherent variability or natural randomness that cannot be reduced. On the other hand, epistemic uncertainty refers to uncertainty that arises due to incomplete or imperfect knowledge (Der Kiureghian & Ditlevsen, 2009). This uncertainty can be attributed to a range of factors, arguably the most important being the imperfect models and associated modelling assumptions; it can be reduced (at least theoretically, and not necessarily in a cost-effective manner) by enhancing our knowledge of the system modelled, e.g., through additional tests.

There are several propagation methods used to assess the uncertainty in the estimates of risk. The choice depends on the complexity of the analysis model, the number and type of input parameters, and the desired accuracy and computational efficiency of the analysis. In current practice, there are two primary approaches that can be identified: a) analytical methods and b) sampling methods.



Analytical methods are mainly based on parametric approximations of the model response and are used to derive approximate closed-form expressions to determine the effect of the propagated uncertainty. Examples include the First-Order Second-Moment method, comprehensively described in the works of Melchers (2002) and Pinto et al. (2004).

In sampling methods, the uncertainty in the system is propagated by generating samples from the input distributions and then numerically evaluating the system response to derive the output distributions. This is the essence of Monte Carlo Simulation (Metropolis & Ulam, 1949) that forms the basis of all such approaches, with the main difference residing in the sampling of the underlying input distributions. Rather than crude random sampling, modern uncertainty propagation approaches conform to the quasi Monte Carlo paradigm, utilizing efficient sampling techniques that aim to achieve better coverage of the sample space with a low number of realizations. The use of Monte Carlo for assessing the safety of a system can be found in all engineering fields, from the assessment of human actions reliability (Vestrucci et al, 1991), to the evaluation of nuclear safety systems (Marseguerra, 2004; Wang, 2018) and the design of LNG fuel gas supply systems (Noh et al., 2014). Among the most commonly employed sampling methods are Latin Hypercube Sampling (LHS, McKay et al. 1979, Iman & Conover 1980), Sobol (1967, 1976, 1979) and Halton (1960) sequences, as discussed in the following sections. Several studies in the past have compared two or more of these approaches, providing recommendations for the selection of an uncertainty propagation method, e.g. Helton & Davis (2003), Briggs (2009), Ellingwood et al. (2009) and Syed & Gupta (2015)). Among them, McKay (1979) has proved that LHS is a better approach than random sampling and a good uncertainty propagation method in general, while Hou et al. (2019) explored the efficiency of quasi-Monte Carlo methods.

## 1.2. Latin Hypercube Sampling

Latin Hypercube sampling is a method of stratified random sampling that guarantees the drawing of each sample from a unique region of the input parameter space. The parameter space is divided into cells conforming to uniform intervals along each axis, and a random sample is drawn from each interval, making sure that it is the only one in each axis-aligned hyperplane containing it (Wikipedia, 2024). By doing so, this method guarantees that the samples are a proper representation of the complete input parameter space, thereby minimizing the possibility of overlooking significant regions.

The combination of Monte Carlo simulation and Latin Hypercube sampling is a robust approach for propagating uncertainty over pure Monte Carlo simulation. This technique comprises generating a significant number of Latin Hypercube samples from the input probability distributions and subsequently utilizing these samples as inputs for the mathematical model or simulation. The obtained output values are employed to approximate the statistical characteristics of the output variables, including mean, variance, and probability of exceedance.

The Latin Hypercube sampling approach (McKay et al. 1979, Iman & Conover 1980) method can be applied to high-dimensional problems, especially after improvements in its sample selection approach (e.g., Dolšek, 2009; Vamvatsikos & Fragiadakis, 2010; Deutsch, 2012; Dige, 2018) to ensure proper coverage with uniform density over the sample space (Owen 1992); notable variants exploit, for example, orthogonal sampling (Tang 1993, Ye 1998).

The steps of Monte Carlo simulation with the CLHS approach for the seismic estimation of model parameter uncertainties are:

1. Define the model, including the input variables (and their distributions) and the expected output variables;
2. Define the sample size  $N$ . It should be sufficiently large to obtain accurate results, but not excessively large to ensure a manageable computational cost.
3. Divide the range of each random input variable into  $N$  equal probability intervals.



4. Randomly (or quasi-randomly) generate one value per interval of each input variable.
5. Combine scalar sample values of the different parameters into  $N$  realization vectors, ensuring that each of the sampled parameter values appears only once in the final sample of  $N$  vectors.
6. Iteratively define  $N$  model realizations by setting model parameters per the sampled vectors, and run the analysis to generate a set of results.
7. Analyze the results to assess the distribution of the output variables.

The problem with the above approach is that if the results are deemed to be of inadequate accuracy, choosing a different  $N$  typically comes at the cost of discarding all previously run analyses. Determining a priori the number of samples to draw is not straightforward, this is why the many authors have proposed a procedure to refine the sampling space, e.g. Tong (2006) and Sallaberry et al. (2008). Progressive/Hierarchical Latin Hypercube Sampling offers a more flexible iterative sampling scheme that retains the structure of LHS. PLHS involves generating samples in successive stages, wherein each stage doubles  $N$ . Thus, one may start with a small enough number of samples that is progressively increased until acceptable accuracy is reached.

According to the methodology proposed by Tong (2006), Sallaberry et al., (2008) and further applied by Vamvatsikos (2014) to IDA for the influence estimation of model parameter uncertainties in earthquake engineering the steps for the application of PLHS are:

1. Define the model, including the input variables (and their distributions) and the expected output variables;
2. Define the initial sample size  $N$ . It should be relatively small to ensure subsequent iterations do not incur an unmanageable computational cost.
3. Divide the range of each random input variable into  $N$  equal probability intervals.
4. Randomly (or quasi-randomly) generate one value per interval of each input variable.
5. Combine scalar sample values of the different parameters into  $N$  realization vectors, ensuring that each of the sampled parameter values appears only once in the final sample of  $N$  vectors.
6. Iteratively define  $N$  model realizations by setting model parameters per the sampled vectors, and run the analysis to generate a set of results.
7. Analyze the results to assess the distribution of the output variables.
8. Double the sample size  $N$ , dividing each parameter interval into equiprobable halves, and create a higher-resolution latin hypercube with half of its cells containing the previous  $N$  observations and the other half being empty.
9. Repeat steps 4-8, filling in the empty cells of the latin hypercube until the desired level of accuracy is achieved.

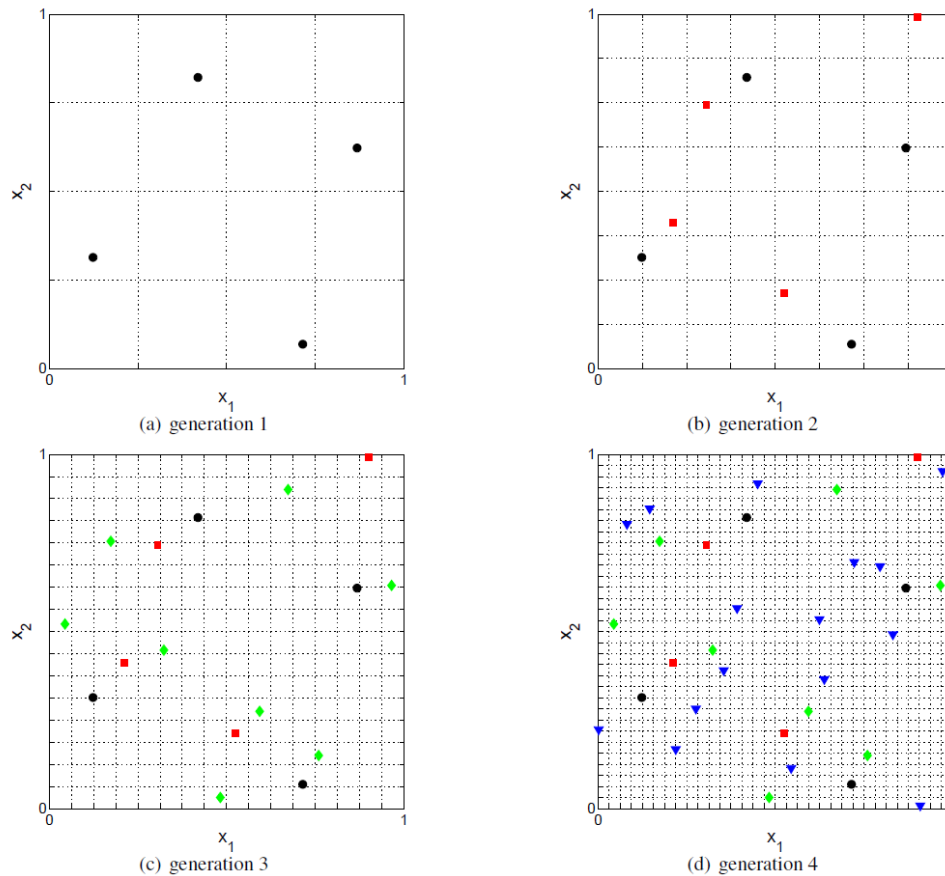


**Figure 1: A progressive LHS design for two uniformly distributed variables is doubled in size by subdividing each stratum to insert new observations: (a) generation 1; (b) generation 2; (c) generation 3; (d) generation 4 (adopted from Vamvatsikos 2014)**

Figure 1 provides an illustrative example of the progressive application of the LHS method. It includes two input variables and begins with an initial small sample size, where  $N$  is equal to 4, and is successively doubled until a satisfactory level of accuracy is reached. In this instance, the equiprobable strata existing along each dimension are subdivided further. This process is repeated three times until a total of four generations have been completed.

In summary, both classic and progressive Latin Hypercube sampling techniques are valuable methods for seismic estimation of structures. The selection of a particular method should be based on the specific requirements of the analysis. Classic LHS is appropriate when a predetermined number of samples is employed and the input space is well-established. In contrast, progressive LHS is more suitable when selecting the sample size should be more flexible.

### 1.3. Sobol sequence

In the realm of quasi-random number generation, Sobol sequences devised by Russian mathematician Ilya M. Sobol in the early 1960s, offer a distinctive approach, particularly valuable when a systematic, low-discrepancy sampling is needed, especially within high-dimensional spaces. The core principle underlying Sobol sequences revolves around generating a sequence of numbers that minimizes the irregularity of points in multidimensional space, thereby optimizing their distribution.

Sobol sequences present several notable advantages. Beyond their low-discrepancy that renders them more advantageous as the dimensionality of the problem space escalates, they guarantee the same sequence when identical parameters are employed, ensuring a uniform and systematic coverage of the sample space. Moreover, they exhibit superior convergence rates compared to entirely random

sequences such as those used in traditional Monte Carlo simulations. This improved convergence enhances the efficiency of simulations and numerical integration.

The fundamental steps for Monte Carlo simulation with Sobol sequence are as follows:

1. Define the model, including the input variables (and their distributions) and the expected output variables;
2. Create a Sobol sequence generator object tailored to the desired number of input variables, e.g. in MATLAB the "sobolset" function is employed;
3. Utilize the Sobol sequence generator to produce  $N$  Sobol sequence points. These generated points will fall within the  $[0, 1)$  interval for each input variable and will be represented as fractions in base 2 (bit sequences).
4. Revert the generated Sobol points to their original distribution space using the transformation equations;
5. Analyze the results to assess the distribution of the output variables.

The suitability of Sobol sequences depends on specific problem characteristics, including the dimensionality ( $s$ ) of the space and available implementation options. As suggested by Fox (1986), for dimensions in the range of  $2 \leq s \leq 6$ , the Sobol generator is recommended, whereas for larger dimensions  $s > 6$  the Faure generator may be a more suitable choice. This recommendation is based on observed performance in terms of speed and accuracy for varying values of dimensionality.

Among the available quasi-random methods are Van der Corput (1935) and Halton (1960) sequences. The Van der Corput sequences are the most basic form of a low-discrepancy sequence. They are created by inverting the digits of a number in base  $b$  and then dividing by  $b$  raised to the power of  $k$ , where  $k$  signifies the digit's location in the number. Figure 2 shows how this type of sequences fill a one-dimensional space taking base 2 as an example. On the other hand, Halton sequences extend the concept of Van der Corput sequences into multiple dimensions, assigning each dimension a distinct prime base in the sequence. However, despite its success in effectively distributing points within lower-dimensional spaces, the Halton sequence faces difficulties in ensuring uniform coverage across higher dimensions when utilizing large prime numbers as bases.

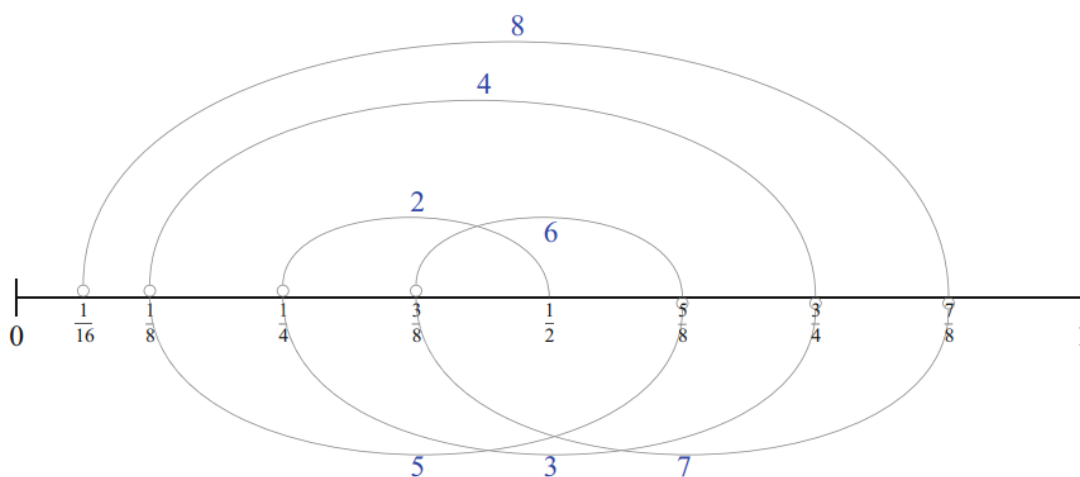


**Figure 2: The first eight points of the base 2 Van der Corput sequences (McClarren, 2018).**



## 1.4. First-Order Second-Moment

The First-Order Second-Moment method is a commonly utilized technique in structural reliability analysis that aims to predict the probability of failure in a system or structure under conditions of uncertainty. It is a straightforward approach that employs the statistical moments of the input variables to estimate the statistical moments of the output variables. Then, based on the first two statistical moments, the method typically calculates the probability of failure. One of the benefits of the FOSM method is its computational efficiency, allowing it to be applied to complex systems or structures with a low number of model evaluations.

The FOSM method employs the chain rule of calculus to derive the first and second-order statistical moments of the output variable from the Taylor series expansion. The first-order moment corresponds to the expected value or mean of the output variable, while the second-order moment corresponds to the variance of the output variable. With these moments estimated, the probability of failure can be computed using the standard normal distribution. However, FOSM method is limited to small variation problems and relatively close-to-linearity problems due to its limitations and that should be carefully considered when applying it to practical problems. First of all, only the first two moments rather than an actual distribution can be assessed for the output, thus typically requiring a normal or lognormal assumption to be made. Additionally, by virtue of using only the linear terms in the Taylor series expansion, the FOSM method will lose accuracy when strong nonlinearity is present. Finally, wherever higher moments become important, FOSM will naturally not be able to follow.

The steps for the application of FOSM approach for the seismic estimation of model parameter uncertainties are:

1. Define the model, including the input variables and the output variables.: Let  $m_{Xk}$  and  $\sigma_{Xk}$ ,  $k=1\dots Z$  be the mean and standard deviation of the  $Z$  input variables;
2. Consider each output variable to be related to the input vector via a function  $f$  approximated through the use of a Taylor expansion;
3. Perform a "Base Case" analysis of the model in which all parameters are set to their mean values. The outputs, or often times their logarithms, are considered a function of the input parameters, e.g.,  $\ln Y^0 = f(m_{X1}, m_{X2}, \dots, m_{XZ})$  in the latter case;
4. Shift each variable from its mean by plus one standard deviation, while all the others are set equal to their mean values;
5. Evaluate the model for the variables defined in step 4 and obtain the output variables of interest as  $\ln Y^{k+} = f(m_{X1}, m_{X2}, \dots, m_{Xk} + \sigma_{Xk}, \dots, m_{XZ})$ ;
6. Shift each variable from its mean by minus one standard deviation, while all the others are set equal to their mean values;
7. Evaluate the model for the variables defined in step 6 and obtain the output variables of interest as  $\ln Y^{k-} = f(m_{X1}, m_{X2}, \dots, m_{Xk} - \sigma_{Xk}, \dots, m_{XZ})$ ;
8. Estimate the first and second moments of each output variable as follows:

$$m_{\ln Y} \approx \ln Y^0 + \frac{1}{2} \sum_{k=1}^Z \frac{\partial^2 f}{\partial X_k^2} \sigma_{X_k}^2 \quad (1)$$

$$\beta_u \approx \sum_{k=1}^Z \left( \frac{\partial f}{\partial X_k} \right)^2 \sigma_{X_k}^2 \quad (2)$$

where the first and the second derivative of  $f$  with respect to  $X_k$  is:

$$\frac{\partial f}{\partial X_k} \approx \frac{\ln Y^{k+} - \ln Y^{k-}}{2\sigma_{X_k}} \quad (3)$$

$$\frac{\partial^2 f}{\partial X_k^2} \approx \frac{\ln Y^{k+} - 2\ln Y^0 + \ln Y^{k-}}{\sigma_{X_k}^2} \quad (4)$$

## 1.5. Comparison of methods

In order to achieve a first comparison between the previously presented methods, 500 random samples are generated Python software (2021). Figure 3 presents the results on a two-dimensional space for pure Monte Carlo, Monte Carlo with Latin Hypercube sampling, Sobol and Halton sequences respectively. It can be observed that, for this number of samples, crude Monte Carlo and Monte Carlo with Latin Hypercube sampling show similar outputs, while for the cases of Sobol and Halton sequences the generated values are more evenly distributed in the sample space covering the empty spaces and avoiding repetitions.

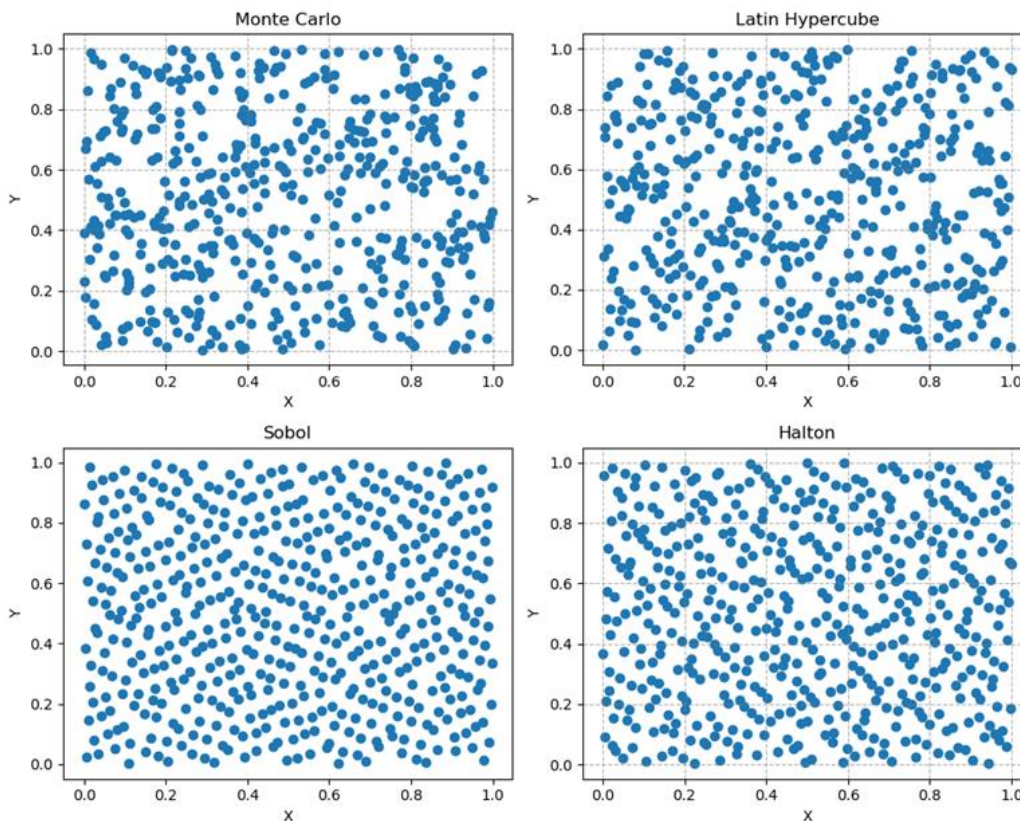


**Figure 3: Filling a two-dimensional space with 500 random samples**

As another illustrative example, a two-dimensional space is created to estimate the value of  $\pi$ . After generating  $10^6$  for each variable,  $x$  and  $y$ , the number  $t$  of values satisfying Equation 5 is calculated. The value of  $\pi$  is calculated by dividing the value of  $t$  by the total number of samples and multiplying the final product by 4.

$$x^2 + y^2 < 1 \quad (5)$$

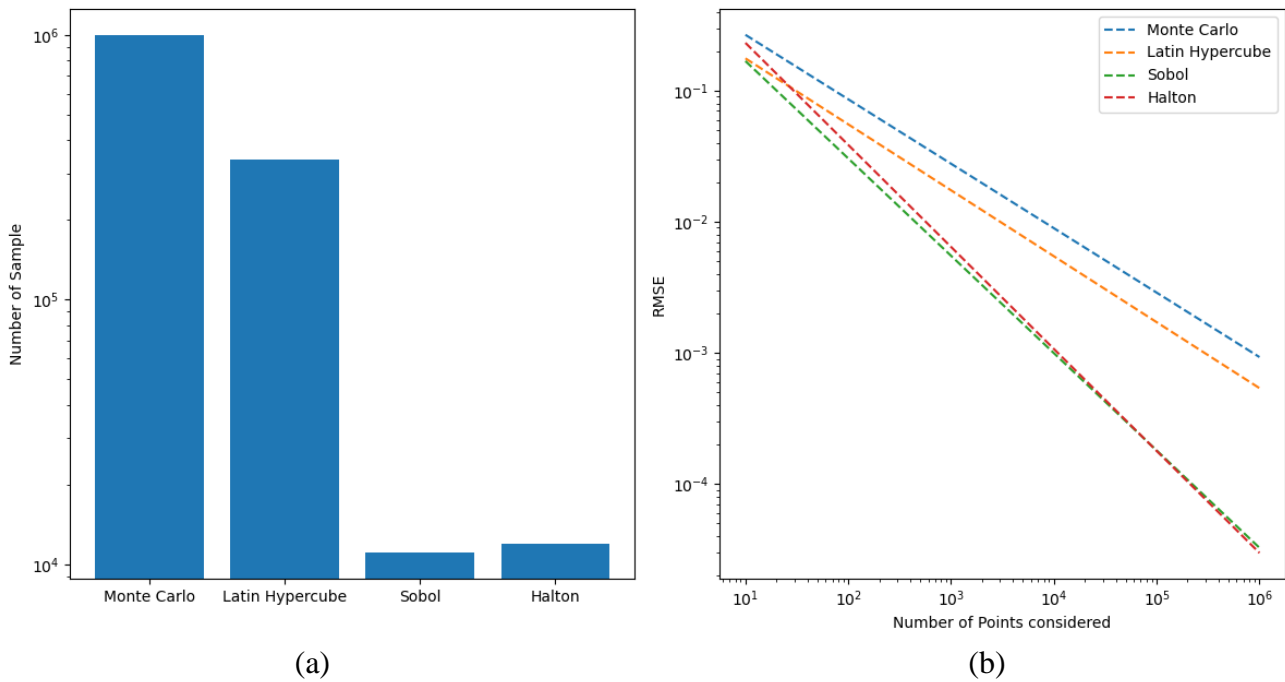


**Figure 4: (a) Comparison of the samples required to achieve the same accuracy (b) comparison of RMSE among different sampling approaches for estimating  $\pi$ .**

Figure 4a illustrates the number of samples required by different sampling approaches to achieve the same level of accuracy, which corresponds to  $10^6$  samples. Figure 4b presents the comparison of the Root Mean Square Error (RMSE) among various sampling approaches for estimating  $\pi$  for a sample size ranging from 10 to  $10^6$ . It is observed that Sobol and Halton sequences show a significant reduction in estimation errors when applied to  $\pi$  calculation methods.



## 2. Uncertainty quantification from literature and recommendations

As presented in the previous section, identifying the input variables is the first step performed in every method. Input variables used to estimate the fragility curves affect the seismic capacity, where capacity factor variables are due to material characteristics, strength equations, and the configuration of the component or structure. When assessing fragility curves based on model analyses, the capacity factor can be calculated in the same general form, or it can be divided into elastic and inelastic parts. If elastic analyses are conducted, the uncertainty related to material resistance is specified in chapter 4 of EPRI (2018), considering the type of materials and failure modes as well as the uncertainty of inelastic energy dissipation in the structure. However, uncertainties related to seismic response, which are mainly due to ground motions, models, and soil-structure interaction are described as follows.

### 2.1. Ground Motion

According to EPRI (2018), when using ground motion response spectra (GMRS) or uniform hazard response spectra (UHRS) as the reference earthquake, it is important to note that the median response spectrum shape variable must be 1.0, with no variation for the effects of randomness or uncertainty. Also, it is possible for the intensity of the ground motion to differ in any arbitrary direction from the two directions selected. As a result, the maximum horizontal response is subject to randomness. The median horizontal peak response factors and logarithmic standard deviations for four commonly used cases are listed in Table 5-4 and Appendix I of EPRI (2018). As reported by Lamprey & Boore (2007), logarithmic standard deviations for the ratio of horizontal spectral acceleration in any arbitrary direction to the geometric mean spectral acceleration for the two horizontal components range from 0.16 to 0.23 for periods from 0 to 1 second.

For Probabilistic Seismic Hazard Analyses (PSHAs), the vertical GMRS or UHRS are derived using site-specific vertical-to-horizontal (V/H) ratios. For the variability of these V/H ratios, a logarithmic standard deviation of 0.25 is typically estimated (EPRI, 2018; ASCE, 2017).

**Table 1: Ground motion variables with their logarithmic standard deviations.**

Ground motion	Variability		Reference
	$\beta_R$	$\beta_U$	
Spectral shape	0	0	EPRI, 2018
	0.14	0	Kim, 2022
	0.15	0.05	Goldschmidt & Sadegh-Azar, 2021
Horizontal direction peak response variability	0.16 to 0.23	0	EPRI, 2018
	0.18	0	ASCE, 2017
	0.10	0	Kim, 2022
Vertical to horizontal (V/H) variability	0.25	0	EPRI, 2018; ASCE, 2017
	0.34	0	Kim 2022

Based on EPRI (1994, 2002, 2009) for the evaluation of the seismic performance of NPP concrete containments, values of 0.14, 0.10, and 0.34 are used as logarithmic standard deviations for spectral shape, horizontal peak response, and vertical peak response, respectively. In addition, for the safety assessment of nuclear facilities, Goldschmidt & Sadegh-Azar (2021) used mean values of  $\beta_R = 0.15$  and  $\beta_U = 0.05$ , respectively. Table 1 shows all the variables related to ground motion with their logarithmic standard deviations based on various references.



## 2.2. Structural damping

For linear dynamic analyses, Table 3-1 of ASCE (2017) provides damping values as a function of the response level and Table 5-6 of EPRI (2018) provides damping values for the median and the median minus one logarithmic standard deviation of the structure. According to Kim et al. (2022) for the epistemic uncertainty on the seismic performance assessment of NPP concrete containments, a median damping ratio of 0.07 and a median minus one standard deviation damping ratio of 0.05 is used. On the other hand, Sadegh-Azar & Hasenbank-Kriegbaum (2014) used a coefficient of variation of 0.35 for damping in the probabilistic seismic analysis of industrial facilities. Standard deviation values for structure damping are presented in Table 2.

**Table 2: Damping variable with its logarithmic standard deviations.**

Structure Response Variable	COV	Reference
Damping	0.35	Sadegh-Azar & Hasenbank-Kriegbaum, 2014

## 2.3. Structural modelling

Variability in structural modelling can be attributed to three key factors, structural frequency, model fidelity, and torsional coupling. The variability of the structural mass is relatively small compared to the structural stiffness (EPRI, 2018). Previous investigations indicate that the coefficient of variation for the ratio of measured to calculated periods, for steel and concrete building types, is about 0.33 (Kennedy et al., 1980; Haviland, 1976; Hadjian et al., 1977). For NPP-type steel or concrete structures, where detailed analyses and accurate models are used, the logarithmic standard deviation for frequency  $\beta_U$  is about 0.15 based on shear wall tests to account for construction materials and connections. As models become cruder the value can be increased to 0.35 for approximate models (EPRI, 2018). Note that these  $\beta$  values correspond to structural frequency and not the variability in response due to variability in frequency.

Model uncertainty or model fidelity refers to how well the model can capture the realistic dynamic response of the structure. Based on EPRI (2018), the logarithmic standard deviation  $\beta_U$  for the additional uncertainty of the model fidelity is estimated to be in the range of 0.05 to 0.15.

Nuclear safety-related structures are analysed using 3D models to consider torsional response, whereas axisymmetric containment structures typically do not exhibit significant torsional behaviour and can be analysed using lumped mass stick models based on EPRI (2018). Kim (2022) used values of 0.17 and 0.06, respectively, for logarithmic standard deviations  $\beta_U$  for modelling frequency and modelling mode shape.

EPRI provides the equipment response standard deviation for a frequency variable between 0.10 and 0.30. For simple equipment analysed by accurate models as well as complex equipment analysed by simpler models the former can be applied (EPRI, 2018). The logarithmic standard deviation for equipment response is typically between 0.05 and 0.15 accounting for uncertainty in the models. Equipment with a single mode of response, which should be the case for most components, a smaller value should be more suitable, while for rigid components this variability should be zero. The larger value should be appropriate for complex equipment (EPRI, 2018). Table 3 and Table 4 show all variables related to modelling with their logarithmic standard deviations for the response of the structure and equipment based on different references.



**Table 3: Modelling variables with their logarithmic standard deviations for structural response.**

Structure Response	Variability		Reference
	$\beta_R$	$\beta_U$	
Frequency	0	0.15 to 0.35	EPRI, 2018
	0	0.17	Kim, 2022
Model fidelity	0	0.05 to 0.15	EPRI, 2018, Goldschmidt et al., 2022
	0	0.06	Kim, 2022
Torsional coupling	0	0	EPRI, 2018

**Table 4: Modelling variables with their logarithmic standard deviations for equipment response.**

Equipment Response	Variability		Reference
	$\beta_R$	$\beta_U$	
Frequency	0	0.10 to 0.3	EPRI, 2018
Model fidelity	0	0.05 to 0.15	EPRI, 2018

## 2.4. Structural response phasing

According to EPRI (2018) when using at least five suites of earthquake acceleration time histories, where the seismic input is the reference earthquake, and averaging their response quantities to obtain a realistic mean phase response with negligible uncertainty,  $\beta_U$  should be considered as zero. However, if a single time history suite is used for the seismic analysis of a structure, it is essential to include the logarithmic standard deviations for both randomness and uncertainty in the time history analysis, with reasonable estimates of  $\beta_R = 0.15$  and  $\beta_U = 0.15$ .

In response spectrum analysis, a reasonable logarithmic standard deviation for randomness in mode combination phasing is  $\beta_R = 0.15$  for structures with multiple important modes, while for simple structures primarily responding in a single mode, a  $\beta_R$  value of 0.05 is considered (Kennedy et al., 1980; EPRI, 2018).

According to EPRI (2018) for equipment with unknown individual modal responses, a range of  $\beta_R$  values from 0.05 to 0.15 can be used. For components analysed using dynamic analyses with few significant modes and larger values for systems with multiple response modes, smaller values are applicable. Table 5 shows all variables related to structure response phasing with their logarithmic standard deviations.

**Table 5: Structure response phasing variables with their logarithmic standard deviations.**

Structure Response Phasing	Variability		Reference
	$\beta_R$	$\beta_U$	
Time-history phasing	Five sets of time histories		EPRI, 2018
	0	Eq. 5-4	
	Single time history		
	0.15	0.15	
Mode combination	0.05 to 0.15	0	EPRI, 2018; Kim, 2022; Kranz et al., 2015

## 2.5. Foundation-Structure interaction

The interaction between the structure and the supporting foundation includes consideration of Ground Motion Incoherence (GMI) and Soil structure interaction (SSI). In general, all foundation considerations affect the response of structures at soil sites, while only GMI has a significant effect at stiff rock sites. Probabilistic response analysis should include soil stiffness and damping as variables in the sampling approach to capture the variability due to uncertainty in SSI analysis. Furthermore, if fixed-base analysis is justified there is no structure response variability due to uncertainty in the soil properties (EPRI, 2018).

Coefficients of variation of the soil properties can be obtained from geotechnical data. If this data is not available, the coefficients of variation of the soil properties can be obtained from the relationship between the median and lower or upper bound values, assuming a lognormal distribution (ASCE, 2017). According to EPRI (2018), when GMI is directly accounted for in the response analysis results, the median response factor is 1.0. The logarithmic standard deviation for uncertainty may be estimated by comparison of Zero Period Accelerations from two SSI analyses using Equation 5, where  $ZPA_{INC}$  corresponds to zero period accelerations from incoherent SSI analysis including GMI effects and  $ZPA_{COH}$  to coherent SSI analysis.

$$\beta_u = \frac{1}{2.5} \cdot \ln \frac{ZPA_{COH}}{ZPA_{INC}} \quad (5)$$

Probabilistic response analysis should include soil stiffness and damping as variables in the sampling to capture variability due to uncertainty in SSI analysis. According to Goldschmidt & Sadegh-Azar (2021), mean values of  $\beta_R = 0$  and  $\beta_U = 0.13$  were used for the SSI variable for assessing the safety of nuclear facilities. Additionally, Kim (2022) used  $\beta_R = 0$  and  $\beta_U = 0.05$  for foundation structure interaction in the study of seismic performance assessment of NPP concrete containments in South Korea. The values reported are shown in Table 6.



**Table 6: Foundation-structure interaction phasing variables with their logarithmic standard deviations.**

Foundation-structure interaction	Variability		Reference
	$\beta_R$	$\beta_U$	
Soil Structure Interaction	0.05	0.13	Goldschmidt & Sadegh-Azar, 2021
	0	0.05	Kim, 2022

## 2.6. Earthquake component combination

Based on ASCE (2017), either the square-root-sum-of-squares (SRSS) method or 100-40-40 method can be used to combine the seismic demands on structural members resulting from three ground motion components. For the combination of earthquake components in building response analysis, a standard value of  $\beta_R = 0.15$  is commonly used for the building eccentricity coefficient (Hadjian et al., 1977).

According to EPRI (2018), for equipment response due to randomness in earthquake component combination, if all three earthquake components contribute approximately equally, a conservative upper limit for  $\beta_R$  is 0.18. If only the two horizontal earthquake components contribute significantly, a logarithmic standard deviation of 0.12 is more reasonable. Earthquake Component Combination (ECC) variability is shown in Table 7 and Table 8 with its logarithmic standard deviations for the response of the structure and equipment, respectively.

**Table 7: Earthquake component combination variable with its logarithmic standard deviations of structural response.**

Structure Response Variable	Variability		Reference
	$\beta_R$	$\beta_U$	
Earthquake component combination	0.18	Based on ECC	EPRI, 2018

**Table 8: Earthquake component combination variable with its logarithmic standard deviations of equipment response.**

Structure Response Variable	Variability		Reference
	$\beta_R$	$\beta_U$	
Earthquake component combination	0.18, for 3 earthquake components	0	EPRI, 2018
	0.12, for 2 horizontal earthquake components	0	EPRI, 2018

## 2.7. Structural response factor of equipment

Based on EPRI (2018) for the equipment fragility, if the structure is in the elastic range the variability is zero. When the equipment is located at or above the structure's center of gravity, logarithmic standard deviations are used to account for variation in seismic demand caused by randomness and uncertainty of  $\beta_R = 0.17$  and  $\beta_U = 0.10$ , respectively (Table 9). If the equipment is mounted in the basement, both values can be set to 0, since the altered structural response should have no or little effect.

**Table 9: Logarithmic standard deviations of equipment response.**

Structure Response Variable	Variability		Reference
	$\beta_R$	$\beta_U$	
Inelastic structure response	0	0	EPRI, 2018 Elastic structural response
	0.17	0.10	EPRI, 2018 Nonlinear structural response and equipment above structure's center of gravity
	0	0	EPRI, 2018 Nonlinear structural response and equipment in the basement

## 3. Implementation case studies

### 3.1. Single degree of freedom system

For the seismic fragility assessment, practice involves the utilization of the Monte Carlo and Latin Hypercube sampling. In order to scrutinize and evaluate the effectiveness of these sampling methods, a simple test case is established. The case under study entails a nonlinear (elastic-hardening) Single Degree of Freedom system (SDoF) subjected to a suite of spectra-fitted synthetic records. The properties of the SDoF are listed in Table 10. The selection of the variability ( $\beta$ ) is informed by the details outlined in Section 2 of this report.

**Table 10: Properties of SDOF**

Properties	Variability	
	Mean Value	$\beta$
Frequency (Hz)	1.00	0.15
Post Stiffness	0.10	0.20
Damping	0.05	0.12
Yielding displacement (m)	0.01	0.20

In this study, to generate the simulated signals, [Seismo Artificial software](#) was utilized by providing a target spectrum selected based on Eurocode regulations (Figure 5). we utilized 500 synthetic ground motion records generated according to specific criteria to faithfully capture the targeted seismic conditions. The target spectra were defined using the EC8 Spectrum with a spectrum factor of 1.0, Peak Ground Acceleration (PGA) of 0.5g, a damping value of 5%, and Type 1 A corresponding to importance class II. The magnitudes of the earthquakes varied between 5 and 8.7, encompassing a range of seismic events. The Joyner-Boore distance was consistently set at 50 km for all records. For accelerogram generation, soil parameters were considered with a shear wave velocity of 940 m/s for stiff rock and 620 m/s for generic rock, ensuring the synthetic records accurately reflected both stiff and generic rock site conditions.

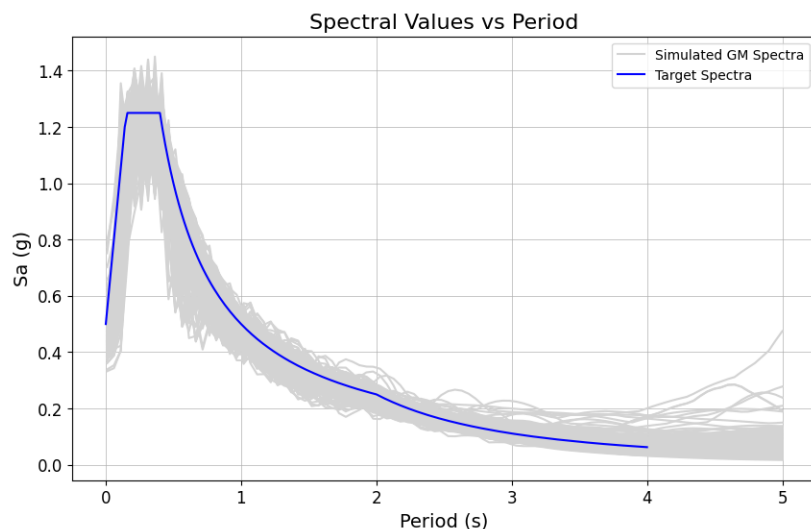


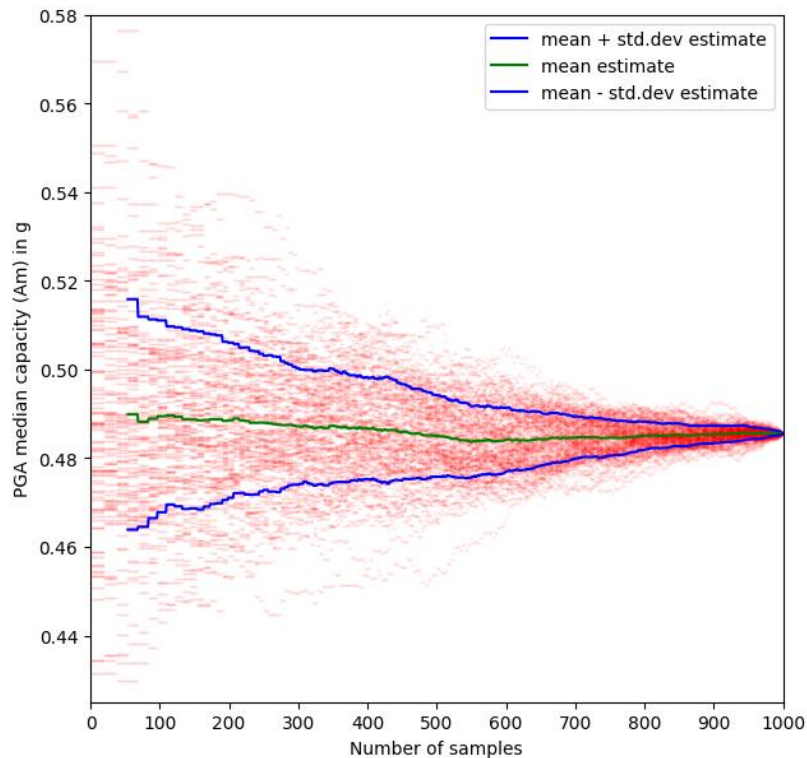
**Figure 5: The target spectra which has been used to generate the simulated signals**

In order to compare the effects of different sampling approaches, crude random sampling is initially executed with  $10^6$  realizations of the model. For each sample an earthquake scenario is randomly

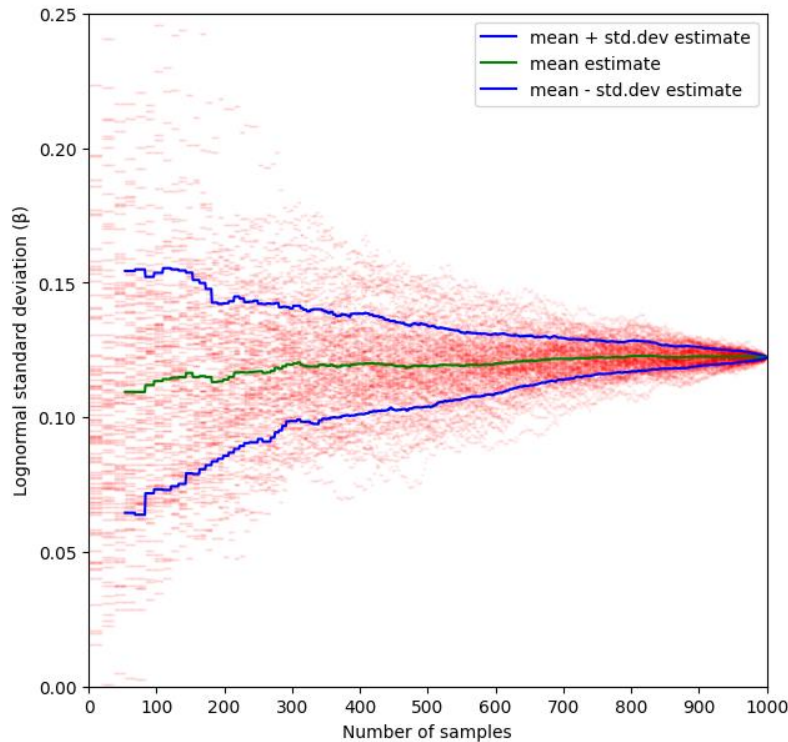


selected. A total of 1,000 samples are generated for Latin Hypercube, Sobol, and Halton sequences, with each sample representing a distinct earthquake scenario. Then, the fragility curve is computed across a range of sample sizes, varying from 10 to 1,000. To make sure to explore the whole search space at each sample size, we divided the search space by the number of samples and forced the algorithm to choose the samples from all the divided spaces. To ensure result stability, this process is repeated 100 times, allowing for an evaluation of the robustness of the predicted curves in relation to the number of calculations.

Cloud analysis is employed to estimate fragility curve parameters. This approach systematically generates synthetic datasets, each simulating the structural response under varying input conditions, such as different ground motion intensities and structural properties. These datasets collectively form a multidimensional "cloud" in parameter space, with each point representing a distinct combination of input variables and resulting structural responses, specifically the displacement of the structure. Statistical regression analysis is then applied to analyse this cloud and deduce the relationship between input variables and fragility curve parameters, such as median capacity and dispersion. By encompassing the entire spectrum of possible scenarios within the cloud, this method offers a robust framework for estimating fragility curves, effectively addressing uncertainties and variability in the structural response.



(a)

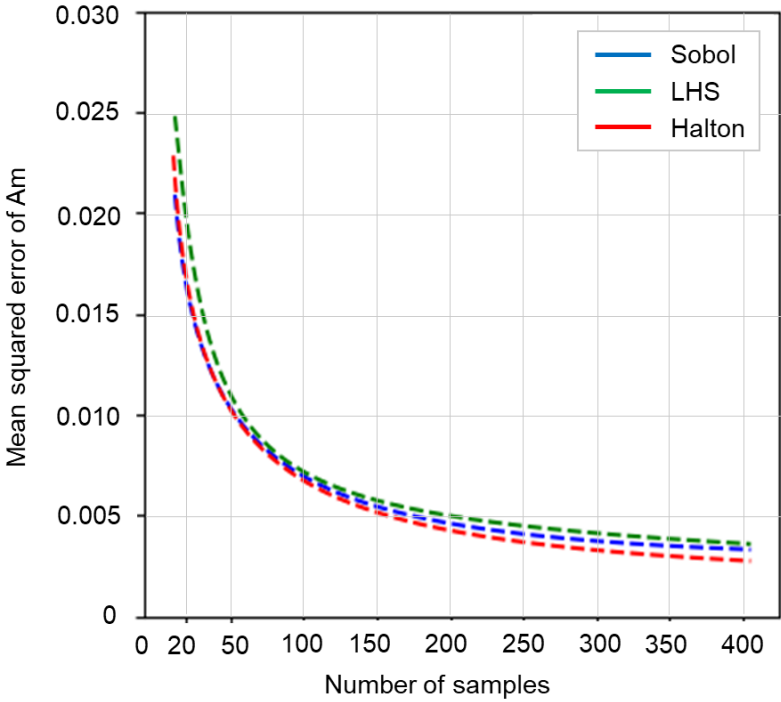


(b)

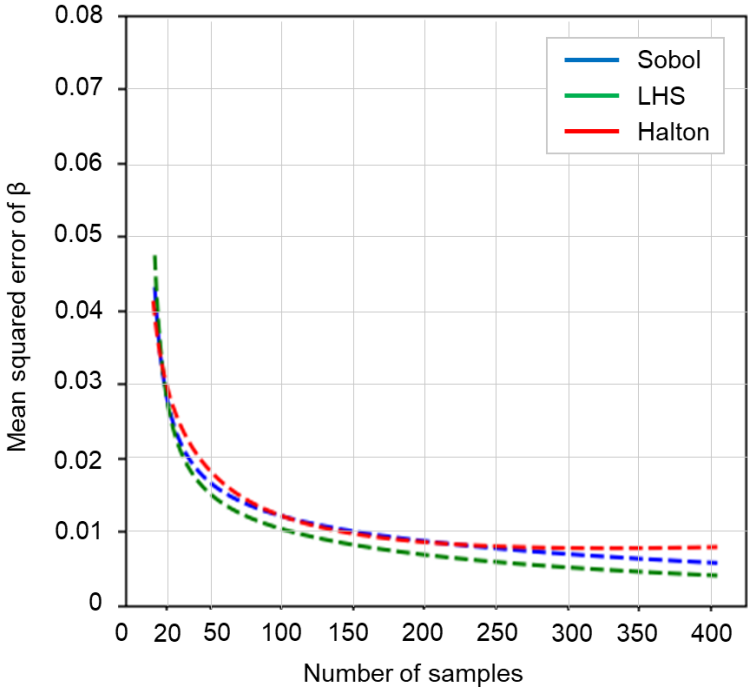
**Figure 6: LHS based fragility parameters  $A_m$  (a) and  $\beta$  (b) depending on the number of samples considered.**

Figure 6 illustrates the variation in fragility parameters estimated by the LHS approach given the number of different samples, where  $A_m$  is the median capacity in terms of PGA and  $\beta$  the logarithmic standard deviation. The scatter points refer to 100 different runs for each number of samples. The green line represents the average value of 100 runs, while the blue lines indicate the average value plus and minus one standard deviation. It is evident from the results of the analyses that the dispersion in estimated fragility parameters diminishes after approximately 300 to 400 samples. This is consistently observed for the Sobol and Halton sequences as well.

Figure 7 depicts the mean squared error values of the estimated fragility parameters for 100 runs and different methods in the initial 400 samples, relative to the Monte Carlo method with 106 samples. Regarding  $A_m$ , the Halton sequence seems to fare slightly better, although there is no significant difference between the three methods. In the case of  $\beta$ , LHS consistently yields the best results. Still, considering the minimal differences in dispersion, along with the random nature of the methods compared, it is challenging to establish any significant superiority among them. Furthermore, it is not obvious if such trends will hold for more complex systems. At the very least, it should be quite obvious that all three improved sampling approaches confer significant advantages relative to crude random sampling.



(a)



(b)

Figure 7: Mean squared error of fragility parameter for 10 to 400 samples for (a)  $A_m$  (b)  $\beta$ .



The estimated fragility curves based on the three sampling approaches and the 400 samples are depicted in Figure 8, compared against the random sampling approach. The graphs illustrate the probability of structure failure given PGA. Notably, all three methods exhibit a commendable level of agreement with the crude Monte Carlo results, showcasing consistency in terms of both average capacity and logarithmic standard deviation. Their performance appears to be approximately equivalent, with Latin Hypercube offering mildly lower median and overall fragility.

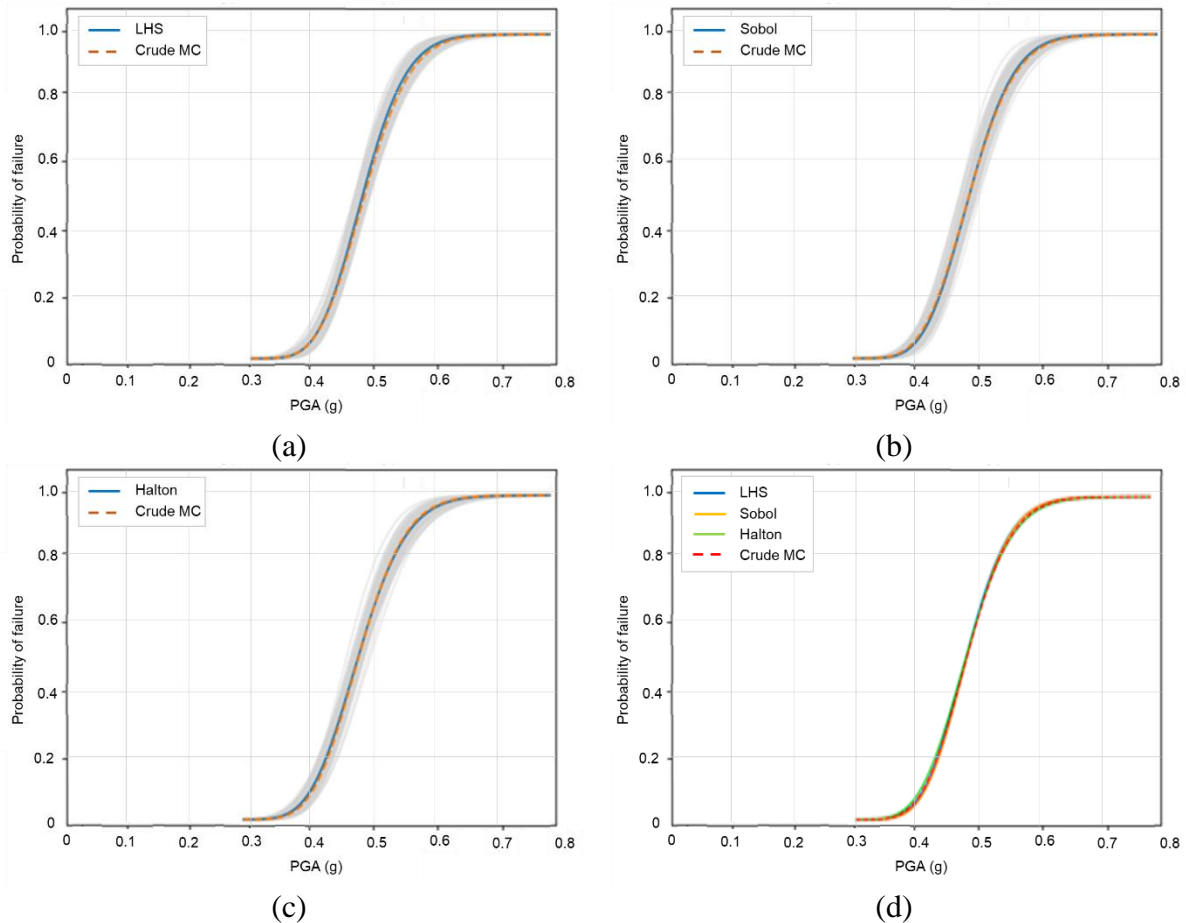


**Figure 8: Fragility curves for (a) LHS, (b) Sobol, (c) Halton, and (d) collectively.**

## 3.2. Pump located on NPP reactor building

### 3.2.1. Model geometry

#### 3.2.1.1. Reactor building

As an additional case study, the main containment/auxiliary building based on the AP1000 advanced reactor design is examined. The AP1000 is an advanced pressurized water reactor (PWR) nuclear power plant design that was developed by Westinghouse Electric Company. It is a third-generation reactor that features a number of safety enhancements over earlier PWR designs, including passive safety systems that require no operator action or electrical power to operate. Some of the safety features of the AP1000 design include a large-volume water tank located above the reactor that can provide a supply of cooling water in the event of a loss of coolant accident, as well as a passive cooling system that uses natural convection to circulate cooling water around the reactor. The AP1000 design has been licensed by the U.S. Nuclear Regulatory Commission (NRC) and has been constructed and operated at several locations around the world.

The structural model, formed using OpenSees (OpenSees, 2006), consists of three concentric sticks with no inter-connectivity at upper elevations (Willaume & Noret, 2011). The sticks represent the Coupled Auxiliary and Shield Building (ASB), the Steel Containment Vessel (SCV), and the Containment Internal Structure (CIS). ASB is a part of a nuclear reactor building that houses auxiliary systems, such as pumps, valves, and electrical equipment. The SCV is a large steel structure that surrounds the reactor pressure vessel. It is designed to withstand high pressures and temperatures that may occur during an accident, and it is often lined with a layer of concrete or other materials to further enhance its strength. CIS, on the other hand, is a system of structural components and support systems that are located within the SCV and helps to support the associated systems.

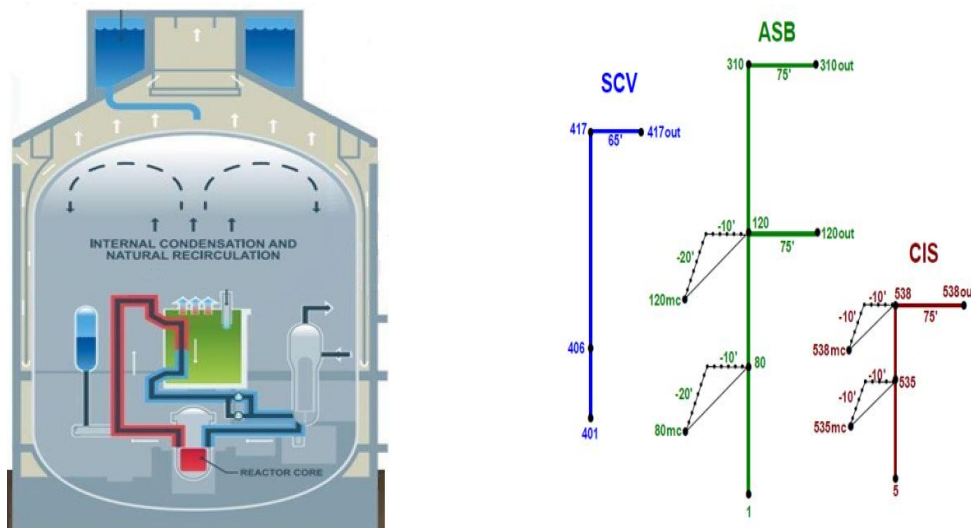


**Figure 9: Original AP1000 reactor design (left) and the corresponding masses-and-sticks model (right) per EPRI (2007).**

The three sticks are horizontally separated in Figure 9 (right), with a concentric and structurally independent arrangement, where each stick comprises discrete masses connected via elastic beam-column elements. The modelling data are taken from the Electrical Power Research Institute (EPRI, 2007). More specifically, the bottom elevations of ASB, SCV, and CIS are 18.44m, 30.48m, and 18.44m in the respective order, and their total heights are 83.10m, 55.44m, and 33.07m. The total mass of the AP1000 is  $1.5 \times 10^5$  tons; the mass ratio of ASB, SCV, and CIS in the entire model is 86%, 3%, and 11%, respectively.

It's important to mention that the EPRI model incorporates massless outrigger nodes connected to the central axis using rigid links positioned at the upper sections of the ASB, SCV, and CIS sticks. To induce natural torsion in the models, the mass centers have been deliberately shifted from the shear center, both within the ASB and the CIS. The shear centers of the three components align along the Z-axis.

The fundamental period of the reference structure, as determined from the modal analysis, is 0.26s. The three substructures exhibit semi-independent vibration behavior, where they are solely connected at the base and do not significantly influence each other; the ASB tower contributes more significantly to the observed vibrational movement of the entire structure. In the reactor building, a stiffness-modifying parameter is utilized as a random variable for the elastic elements. This variable is assumed to be uniformly applied to all structural elements, exhibiting perfect positive spatial correlation. The random variable for the stiffness modifying parameter of the reactor building is modelled as following a lognormal distribution with a dispersion of 0.50.

### 3.2.1.2. Soil structure interaction

The inclusion of soil-structure interaction (SSI) is an essential aspect in the assessment of the seismic safety of a nuclear power plant. A simple cone model is utilized to replicate the interaction between the soil and the structure-foundation system. The first attempt to create a simple physical model of soil can be traced back to Ehlers (1942), and subsequently, Wolf (1998) employed a truncated semi-infinite cone to depict the vertical and horizontal movements of a foundation located on an elastic half-space. Various samples of cones representing vertical, horizontal, rocking, and torsional degrees of freedom are presented in Figure 10. According to Wolf, a rigid basemat on the surface of a homogeneous soil halfspace with Poisson's ratio  $\nu$ , can be modeled for all components of motion as a truncated semi-infinite cone of equivalent radius  $r_0$ , apex height  $z_0$  and wave velocity  $C$ . For the horizontal and torsional cones deforming in shear the appropriate wave velocity,  $C$  equals the shear-wave velocity  $C_s$ . For the vertical and rocking cones deforming axially,  $C$  equals the dilatational-wave velocity  $C_p$  for  $\nu \leq 1/3$  and is limited to  $2C_s$  for  $1/3 < \nu \leq 1/2$ .

From a modelling perspective, the cone is represented as a lumped-parameter mass-spring-damper system. The underlying assumption of the model is that the soil can be approximated as a linear elastic medium with uniform stiffness throughout its depth. The foundation of the structure is illustrated as a rigid mass that is linked to the soil through a spring and a dashpot (Figure 11). The spring represents the stiffness of the soil, while the dashpot incorporates the damping characteristics of the soil. A rectangular foundation with a plan dimension of 65×45m, roughly representative of the AP1000, is utilized for the analysis. Also, a shear wave velocity of 350m/s and a density of 2Mgr/m<sup>3</sup> are assumed for the soil. The fundamental period of the powerplant, considering the mass-spring-damper system for the SSI, is equal to  $T_1 = 0.46s$ , while the second and third modes come at  $T_2 = 0.31s$ , and  $T_3 = 0.30s$ . At even shorter periods we encounter the vibration modes of the three substructures, which in the presence of SSI vibrate semi-independently, each one only connected to the others at the base. The fundamental periods of the ASB, CIS, and SCV towers now become  $T_{ASB} = 0.39s$ ,  $T_{CIS} = 0.29s$ , and  $T_{SCV} = 0.15s$ , respectively. Rayleigh damping of 7% (per ASCE, 2019) is applied to the 1<sup>st</sup> and 3<sup>rd</sup> global structural modes, i.e., at periods of 0.46s and 0.30s. In order to propagate the uncertainty of the cone model, a stiffness-modifying parameter is employed as a random variable for the soil cone model. The stiffness-modifying parameter of the soil also follows a lognormal distribution with a dispersion of 0.50.

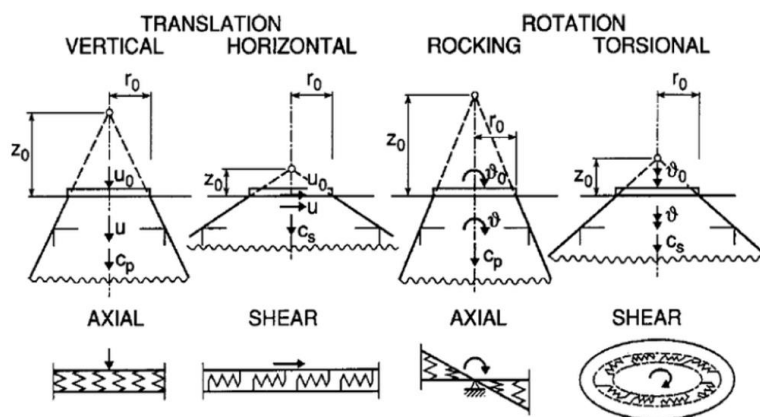
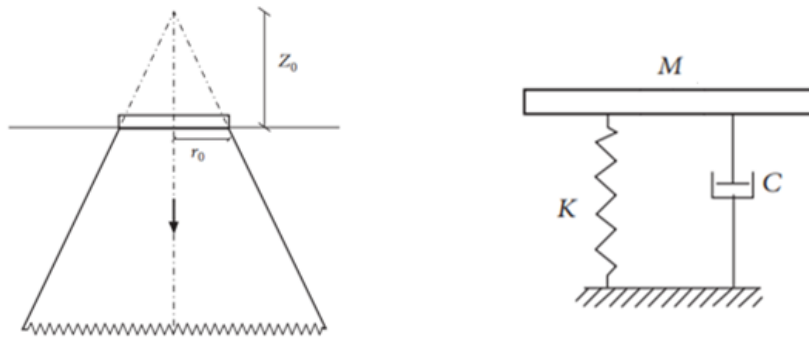


Figure 10: Cones for different degrees of freedom (Wolf, 1998).



**Figure 11: Cone model (left) and mass-spring-damper system (right).**

### 3.2.1.3. Service water pump

Non-structural components in nuclear power plants refer to equipment, systems, and components that are not integral parts of the primary structures, but are crucial for ensuring the safe and dependable operation of the facility. These components comprise pumps, valves, electrical and instrumentation systems, as well as HVAC (heating, ventilation, and air conditioning) systems. Seismic risk assessment of nuclear power plants necessitates the assessment of potential earthquake impacts on both the structural and non-structural components. While the structural components are designed to resist seismic forces, non-structural components are susceptible to damage or failure during an earthquake due to their location, mass, and interaction with the structure. The failure of non-structural components can potentially cause secondary hazards like fires, flooding, or radiation leaks, which can significantly affect the safety of the plant and the surrounding community. Therefore, it is essential to evaluate and assess the seismic vulnerability of non-structural components to ensure the overall safety and reliability of nuclear power plants.

To perform a reliability analysis, a service water pump (EPRI, 2018) is used as an example case study, with particular emphasis on the motor stand (Figure 12). According to the EPRI (2018) report, the translation of the pump motor is one of the most critical failure modes; therefore, the focus shifts to the motor stand. The motor stand has a cylindrical shape with two large windows cut out, resulting in two 120° arcs that act as guided cantilever beams in bending about the weak axis direction when lateral acceleration is applied to the motor. The pump dimensions adopted in EPRI (2018) are smaller than what would normally be employed, resulting in a significantly more flexible motor stand. The simplified model (Figure 13) used for the simulation is a three-dimensional stick, which incorporates a single mass situated at its upper end. It is assumed to be positioned on the top floor of the CIS tower.

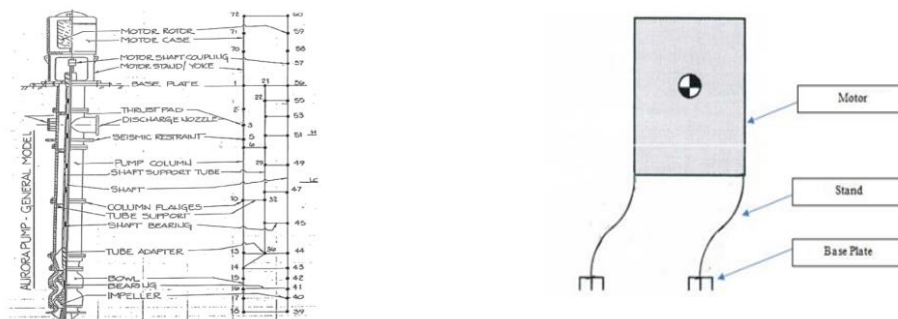


**Figure 12: Original model of the service water pump (left) and simplified motor stand model per EPRI (2018) (right)**

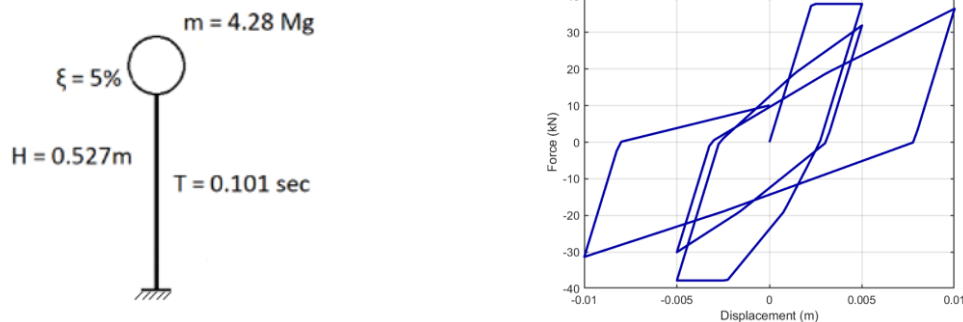


**Figure 13: Pump motor stand model (left) and hysteretic behavior of the model under static cyclic loading (right).**

The pump's performance, illustrated in the right part of Figure 13, is characterized by an elastic-perfectly-plastic force-deformation backbone that ends at an ultimate ductility of 1.25 and exhibits moderately pinching hysteresis. When uncertainties are ignored, the pump is symmetric in both principal axes X and Y and has a fundamental period of  $T_{\text{pump}} = 0.101\text{s}$  and a yield strength of  $V_{\text{yield}} = 37.79\text{kN}$ . A median damping ratio of  $\zeta = 5\%$ , typical for mechanical equipment (as stated in EPRI 2018), is adopted. Failure takes place at a maximum displacement of  $d_u = 0.0029\text{m}$  for the pump; this the displacement where the pump axle exceeds its operational tolerances, and it is utilized as the capacity threshold for fragility analysis. Five random variables are employed to describe the component features, including the damping ratio, fundamental eigenperiods, and yield strengths in the two principal axes ( $\zeta_{\text{pump}}, T_{\text{pump},x}, T_{\text{pump},y}, V_{\text{yield},x}, V_{\text{yield},y}$ ). Each of these parameters follows a lognormal distribution with the median value described previously. The yield capacity, damping, and component period have dispersions of 0.16, 0.12, and 0.18, respectively.

## 3.2.2. Performance evaluation

### 3.2.2.1. Uncertainty analysis

The reactor building and the pump are analysed independently. Given the significantly lower mass of the pump relative to the reactor building, a two-stage cascade approach is employed for the analysis. By adopting this cascading approach, a significant reduction in computational time is achieved during the uncertainty analysis, as it allows us to sample and analyse the reactor structure and the pump separately. For the first, we employ LHS, in MATLAB (MathWorks, 2023) programming language, to sample realizations of the reactor structure varying the stiffness factors for the structural members and the mass-spring-damper system employed for SSI (Table 11). Given that the model only has few degrees of freedom, and the stiffness of the elements is perfectly correlated, only 12 instances are employed for the elastic model of the reactor building. These are enough to achieve errors less than 5% in both the mean and the standard deviation of the first-mode period with respect to the actual "population" value (estimated for a sample of >100 realizations). The resulting dispersion in the first-mode period of the reactor building ( $T_1$ ) is 0.20, matching the values reported in EPRI (2018). To propagate the parametric uncertainty from the structure to the pump domain, two distinct approaches are employed, namely Monte Carlo simulation and FOSM. For Monte Carlo, the samples of the parameters governing the behavior of the pump are generated using classic LHS, progressive LHS and Sobol sequences.

Monte Carlo simulation with classic LHS method involves generating a Latin hypercube of random samples of the random parameters. Herein, 50 realizations of the pump model are drawn via LHS. Additionally, the heuristic approach proposed by Charmpis & Panteli (2004) is applied to rearrange the samples and impose zero correlation among the five random variables of the pump. The optimization



algorithm employs an objective function to measure the difference between the intended and actual correlations. This metric of dissimilarity is expressed mathematically as the Root Mean Square Error (RMSE), which was introduced by Lurie and Goldberg in 1998. In this specific instance, the RMSE is less than 1%.

On the other hand, Monte Carlo simulation with progressive LHS is an extension of classic LHS that permits the sequential refinement of the sample. Seven iterations are executed to achieve comparable outcomes to classic LHS. Starting with a size of 10 realizations for the first generation, after  $M$  iterations (or generations), the sample size becomes  $10 \times 2^{M-1}$ . For  $M = 8$  this results in 1,280 model instances in the final generation. Although this is far larger than the 50 of CLHS, in the latter case we employ 30 ground motion records per each model realization, for a total of  $30 \times 50 = 1,500$  record-model combinations. In the context of record-wise PLHS, each model is paired with only one ground motion record at a time, rather than an entire set of records, thus CLHS and PLHS are on par in terms of computational cost. In each sample, the rearrangement algorithm of Charmpis & Panteli (2004) is employed to eliminate any spurious correlations, attaining an RMSE below 1%.

In the framework of the Sobol sequence method, 125 distinct pump model realizations are generated, each to be analysed under 30 ground motion records; no inherent correlation is introduced among the samples. RMSE is employed to assess the discrepancy of sample correlations and a desired zero correlation target. Due to the stricter approach of generating the Sobol samples, rearrangement cannot be employed. Thus the 125 realizations were required to ensure RMSE of the order of 10% is achieved.

**Table 11: Stiffness-modification factors for the reactor building and the soil and the corresponding fundamental period of the model per each of 12 LHS realizations.**

Model realization	Stiffness-modifying parameters		$T_1$ (s)
	Reactor Building	Soil	
1	0.486	0.807	0.53
2	1.425	0.736	0.51
3	0.904	1.409	0.40
4	1.675	1.187	0.41
5	0.682	2.158	0.37
6	0.979	0.364	0.72
7	0.524	0.558	0.61
8	0.837	1.042	0.46
9	1.110	1.283	0.41
10	2.111	0.613	0.55
11	1.229	1.704	0.36
12	0.710	0.915	0.49

To apply the FOSM method,  $2 \times Z + 1 = 11$  simulations are required, where  $Z = 5$  is the number of random variables. The first simulation involves setting all random variables to their mean values. Then plus/minus perturbations of each parameter are employed. Simulations  $i = 2, \dots, 6$ , are obtained by shifting each parameter from its mean by plus one standard deviation, while the other variables remain constant at their mean values. The remaining simulations,  $i = 7, \dots, 11$ , use mean values minus one standard deviation instead.

### 3.2.2.2. Dynamic analysis

All of the aforementioned methods for uncertainty propagation are integrated within the framework of Incremental Dynamic Analysis (IDA, Vamvatsikos & Cornell, 2002). A set of 30 "ordinary" (i.e. non-pulse like, non-long duration) natural ground motion records was selected from the NGA-West2 database (Ancheta et al., 2013) for evaluating the induced seismic demands via IDA, considering the horizontal components of the excitation in both orthogonal directions. The record selection process is documented



by Bakalis et al. (2018), where the interested reader could find more details on how the hazard-consistent ground motions were selected using the conditional spectrum record selection technique proposed by Kohrangi et al. (2017). The conditioning IM is Average Spectral Acceleration (AvgSa) in the range from 0.1 to 1.0 with an increment of 0.1sec, using the geomean of both ground motion components for each spectral ordinate. Selection was performed via the Jayaram et al. (2011) algorithm for the 2% in 50yrs hazard level. The record sequence numbers (RSN) of the selected ground motions are as follows: 33, 163, 231, 316, 371, 411, 728, 745, 802, 825, 855, 880, 1077, 1177, 1202, 1234, 1259, 1268, 1277, 1503, 1507, 1549, 1596, 1617, 1787, 2654, 2703, 2893, 3222, 3512.

In the first stage of the two-stage cascade approach for the analyses of the reactor building and the pump, a dynamic analysis is carried out for every alternate model of the reactor building and the soil-foundation system. Under the assumption of linear elasticity, the floor acceleration time histories obtained from these analyses can be scaled to obtain the response at various scaled intensity levels of the ground motion records. By employing this approach, a second-stage IDA is conducted to assess the performance of the pump.

The first model, referred to as the "R2R only" sets all parameters at their mean values, resulting in the record-to-record variability (R2R) being the only source of uncertainty. The analysis involved a total of  $12 \times 1 \times 30 = 360$  IDAs, where each realization of the structure is paired with the single model realization of the pump under the influence of the entire set of 30 two-component floor motion records.

Subsequently, the CLHS-based Monte Carlo simulation involved a total of  $12 \times 50 \times 30 = 18,000$  IDAs, where now 50 pump model realizations are involved. In the case of the Sobol sequence-based Monte Carlo simulation, the total number of IDAs is equal to  $12 \times 125 \times 30 = 45,000$ . As discussed earlier, the record-wise application of PLHS application involved the use of a single two-component floor motion record per model realization, whereby the first model is paired with the first record, the second model with the second record, and so forth, cycling back to the first record after every 30 model realizations. This approach resulted in  $12 \times 1,280 \times 1 = 15,360$  IDAs. In contrast, FOSM required the use of the entire floor motion set per each perturbed model, resulting in  $12 \times 11 \times 30 = 3,960$  IDAs. All cases are illustrated in Table 12.

**Table 12: Number of analyses of the reactor building and the pump and number of records leading to number of IDAs performed.**

Method	Reactor building realizations	Pump realizations	Number of records per realization	Number of IDAs
R2R only	12	1	30	360
CLHS	12	50	30	18,000
PLHS	12	1280	1	15,360
Sobol	12	125	30	45,000
FOSM	12	11	30	3,960

Usually, a single scalar is utilized to characterize a ground motion record, and its selection is critical since it serves as the sole connection between seismic hazard and structural response. This scalar is known as the intensity measure and must possess certain characteristics. It should be general enough to allow for the computation of its hazard through an appropriate ground motion prediction model, while also being specific enough to be closely related to the response of the structures, systems, and components of the power plant.

Given these requirements, three potential scalar IMs are considered. The first is PGA, which is widely used in the nuclear industry (e.g. Zentner et al., 2011). The second scalar IM under examination is the 5%-damped spectral acceleration at a specific period T, or Sa(T), which is deemed an appropriate index for first-mode-dominated linear or nonlinear structures. Finally, the AvgSa in distinct ranges of short periods is considered, as it has been demonstrated to deliver satisfactory performance for a variety of



structures (Vamvatsikos & Cornell, 2005; Bojórquez & Iervolino, 2011; De Biasio et al, 2014; Eads et al., 2015; Kazantzi & Vamvatsikos, 2015; Kohrangi et al., 2016; Adam et al., 2017, Zentner et al, 2017). To ensure consistency with contemporary ground motion prediction equations, the geometric mean of the two horizontal ground motion components is utilized to define all three types, rather than the arbitrary or maximum component value.

Note that herein, we only seek to employ uncertainty propagation techniques to investigate the effect of parameter uncertainty on the IM optimality. Therefore, we are only employing a limited set of potential IMs. Beyond PGA, Sa is defined at the fundamental period of the pump ( $T_{\text{pump}} = 0.101\text{s}$ ). Additionally, three distinct period ranges are considered for AvgSa, namely (0.10-0.40s), (0.10-0.20s), and (0.05-0.15s). A more comprehensive investigation of IMs suitable for use in nuclear power plants is presented in METIS Deliverable D6.3 (Dolšek et al., 2024).

The displacement response of the 3D service water pump model includes two horizontal components, labeled as X and Y. To estimate the structural response of the model, the Engineering Demand Parameter (EDP) is calculated by identifying the maximum value (over time) of the geometric mean of the X and Y displacement time histories.

### 3.2.2.3. Fragility analysis

After the incremental dynamic analyses are performed, the results are utilized to obtain fragility functions of the pump per Bakalis & Vamvatsikos (2018) using the so-called vertical statistics approach. Essentially, for each IDA curve generated by a single-record, the IM value that corresponds to the given limit-state threshold of 0.0029m is estimated. Then, the fragility curve is simply the Cumulative Distribution Function (CDF) characterizing the IM values derived from the pertinent set of IDAs. This could be either a non-parametric empirical CDF, or a fitted parametric one. Since FOSM can only estimate the first two moments of the fragility curve, and given that a lognormal CDF is the most typical fragility model employed, we choose to fit a lognormal even in the case of the Monte Carlo based approaches, achieving a common basis for comparison.

The subsequent step for the "R2R only" and the Monte Carlo based approaches, involves estimating the lognormal distribution parameters, i.e., the median and the logarithmic standard deviation of the pertinent IM-values. To estimate the median IM and dispersion resulting from parameter uncertainty using the FOSM method, Equations 1-4 outlined in Section 1.4 are utilized. The SRSS approach is employed to combine the record-to-record dispersion estimated by the "R2R only" investigation with the additional dispersion caused by parameter uncertainty, in the case of the FOSM method.

The process of deriving fragility functions is conducted for the three different types of IMs, i.e.,  $S_a(T,5\%)$ , PGA, and AvgSa. Table 13 contains the median ( $\mu$ ) and Table 14 the lognormal standard deviation ( $\beta$ ) of each fragility analysis performed conditioned on the examined IMs.

**Table 13: Medians of fragility curves given the IM for the R2R only analysis versus the three uncertainty propagation methods. All values in units of g.**

Method	PGA	Sa(0.101s)	AvgSa(0.1-0.4s)	AvgSa(0.1-0.2s)	AvgSa(0.05-0.15s)
R2R only	0.43	0.72	0.86	0.86	0.70
CLHS	0.38	0.63	0.76	0.75	0.62
PLHS	0.39	0.64	0.77	0.76	0.63
Sobol	0.38	0.64	0.77	0.76	0.62
FOSM	0.36	0.63	0.79	0.73	0.61



**Table 14: Dispersions of fragility curves given the IM for the R2R only analysis versus the three uncertainty propagation methods.**

Method	PGA	Sa(0.101s)	AvgSa(0.1-0.4s)	AvgSa(0.1-0.2s)	AvgSa(0.05-0.15s)
R2R only	0.30	0.12	0.30	0.18	0.17
CLHS	0.31	0.24	0.31	0.25	0.23
PLHS	0.30	0.24	0.30	0.24	0.23
Sobol	0.31	0.23	0.31	0.25	0.23
FOSM	0.35	0.21	0.34	0.25	0.25

Henceforth, the comparison is twofold. First, we are interesting in potential biases in the median and dispersion estimates due to the different methods employed, thus comparing *vertically* within each column of Table 13 and Table 14. Second, we want to look at the effect of the IM on the dispersion estimates, therefore comparing *horizontally* across rows of Table 14 to figure out the achieved efficiency.

In terms of bias, the medians of Table 13 clearly indicate that neglecting parameter uncertainty is lowering the overall capacity. The R2R only shows higher medians across all IMs, while the three Monte Carlo approaches achieve similar results. FOSM shows mild deviations with respect to the latter, sometimes coming higher and sometimes lower than Monte Carlo, but always less than the "R2R only" case where pump uncertainty is neglected. In terms of dispersion, all uncertainty propagation methods achieve similar results, with FOSM sometimes coming a bit higher and sometimes a bit lower than the rest. The most interesting comparison is against the R2R only. Interestingly enough, when the IM has low efficiency, as for example PGA or AvgSa(0.1-0.4s), then the added parameter uncertainty has little effect: 30% for the R2R only versus 30-31% for the Monte Carlo approaches. For more efficient IMs, e.g., Sa(0.101s), AvgSa(0.1-0.2s), and AvgSa(0.05-0.15s), the effect of the uncertain parameters becomes more prominent: 0.12 to 0.18 dispersion without parameter uncertainty becomes 0.23 to 0.25 with uncertainty included. It should be expected that such differences will be enlarged for both efficient and less efficient IMs when more complex models with numerous uncertain parameters are investigated, as typical of nuclear power plants.

Figure 14 depicts the dispersion of spectral acceleration values over a range of periods from 0 to 0.5s. Horizontal lines are also plotted to represent dispersions for AvgSa(0.10-0.40s), AvgSa(0.10-0.20s), and AvgSa(0.05-0.15s); all results correspond to Monte Carlo simulations with PLHS. The fragility dispersions for PGA (found at the zero-period acceleration) and AvgSa(0.10-0.40s) are similar, as discussed earlier. Spectral acceleration offers lower or equivalent dispersions for periods within [0,0.20s], with the lowest value of  $\sim 0.24$  reached at the period of the pump. Still, this single period would only work for this particular component. If other equipment at different fundamental periods were shown, one can visualize their performance via "lateral transpositions" of the Sa(T,5%) curve centered at said component periods. Instead, AvgSa(0.10-0.20s) and AvgSa(0.05-0.15s) show almost equally good dispersions (the latter being the overall optimal), while not being tied to any specific period. It is conceivable that selecting Sa at any period may be less effective for a set of components than averaging over a period range, unless all components are closely grouped together in terms of period.

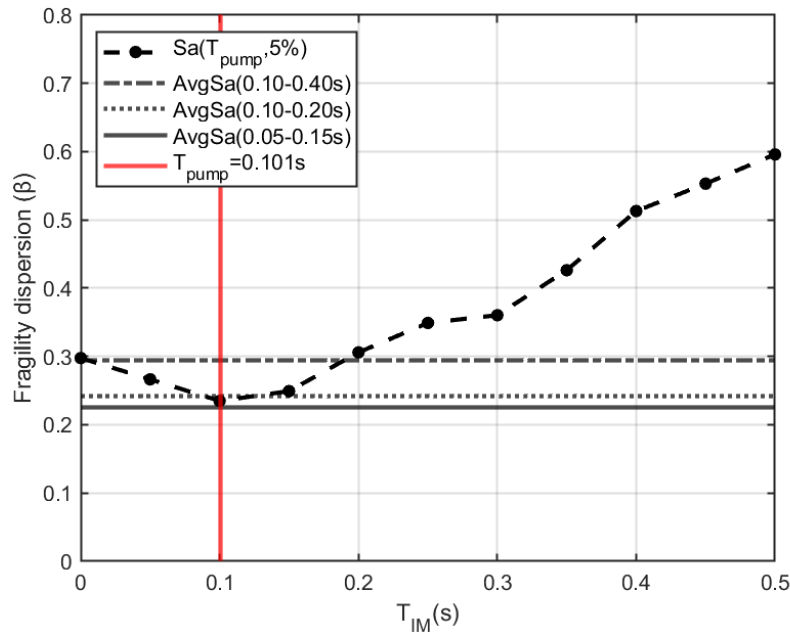


**Figure 14: Distribution of dispersion for Sa over a range of periods from 0 to 0.5s. “Period-independent” dispersions for AvgSa(0.1-0.4s), AvgSa(0.1-0.2s) and AvgSa(0.05-0.15s) are also indicated with straight lines.**

Considering the similar outcomes of the four uncertainty propagation approaches, at least for the case at hands, it makes sense to focus on the computational resources expended in each case. Obviously, the time required for conducting these analyses is contingent upon the total number of samples. Monte Carlo simulation with CLHS requires 20 hours to complete, while PLHS needs only 18 hours. Of course, this is a direct outcome of employing 1,500 versus 1,280 IDA curves, i.e., it depends on the analyst’s choices rather than any inherent characteristic of each method. One might have chosen to employ only 1,000 IDA curves for CLHS, theoretically beating PLHS. The real difference is that this number has to be selected a priori for CLHS while it is iteratively reached in PLHS. In other words, PLHS has a better chance of economizing on runs if the required accuracy is reached early in the iterative algorithm. CLHS can match this performance only if one has the experience to pre-select the right number of samples. Sobol sequences took approximately 50 hours. This is a direct consequence of requiring a larger sample to reduce spurious correlations. For larger problems and, per chance, by employing other correlation-setting approaches, this issue can be mitigated without trouble. Finally, utilizing the FOSM technique involves only 11 perturbed models of the pump, with the analysis being completed in only about 5 hours. However, it’s essential to emphasize that the relatively low number of required analyses is heavily problem dependent. If the number of these uncertain parameters increases, both the total number of analyses and the computation time will inevitably rise as well, in some cases easily exceeding the totals of CLHS and PLHS as each random parameter will always require two perturbed models to be considered.

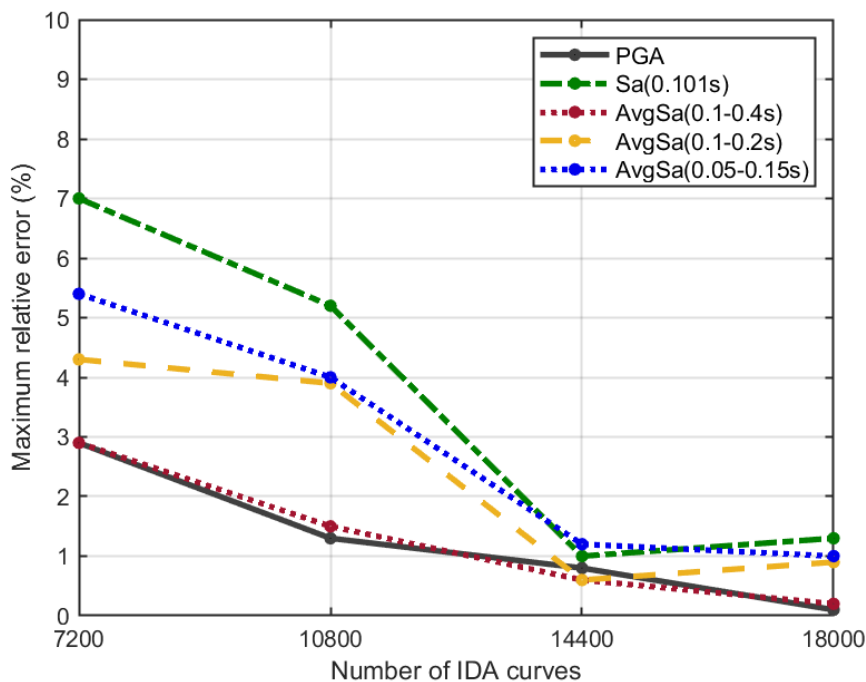
Overall, a significant challenge revolves around determining the appropriate number of analyses to perform. One potential solution is to initially set a relatively large number and employ a stopping criterion that can expedite the procedure. As a result, a straightforward rule can be established using the relative changes in estimated IM values at the given EDP. Let  $\Delta\mu_{IM|EDP}$  and  $\Delta\beta_{IM|EDP}$  denote the relative changes in the median and dispersion of the IM capacity for different numbers of samples/generations. A robust stopping criterion can be constructed by mandating that the maximum value, among  $\Delta\mu_{IM|EDP}$  and  $\Delta\beta_{IM|EDP}$ , satisfies a specific tolerance, e.g. declaring that sufficient convergence has been achieved when the results of successive sample sizes differ by 5% or less.



Figure 15 illustrates the maximum relative error for different analysis steps, which is equivalent to the number of IDAs performed for the pump using the CLHS method. It's evident that the results vary among the various IMs employed. Specifically, PGA and AvgSa(0.1-0.4s) exhibit a quicker convergence compared to the other IMs, requiring a lower number of analyses. Actually, these non-optimal IMs essentially only need the median to converge, rather than the more troublesome dispersion (which is not influenced by the low added uncertainty). This convergence is achieved much faster, reaching a relative error of only 3% with 7,200 IDAs. The more efficient IMs, and especially Sa(0.101s), have a lot more ground to cover in the slow-converging dispersion, therefore they require at least  $12 \times 30 \times 30 = 10,800$  IDAs, or 30 pump realizations, for a  $\sim 5\%$  tolerance; the total analysis time runs to 12 hours. Note that a record-wise application of CLHS, akin to PLHS, would offer a better parameter sampling scheme, involving more pump realizations and probably a better convergence rate.

When estimating the same results, as shown in Figure 16, for Monte Carlo simulation using the Sobol sequence, it demonstrates an overall strong performance, regardless of the selected IM. Considering a tolerance of 5% as few as 7,200 IDAs, which correspond to 20 pump model analyses, would suffice to generate the fragility parameters for the pump, resulting to an analysis time equal to 8 hours. The same argument in favour of a record-wise application made earlier, also applies for the Sobol approach.

Finally, the flexibility of the PLHS approach becomes apparent in Figure 17. Therein, executing 320 pump model analyses, or alternatively 3,840 IDAs, would mean reaching a 5% tolerance in a timespan of less than 5 hours, offering the fastest overall approach. As expected, though, one needs to be careful not to terminate the algorithm early as there is significant variability in the early generations.



**Figure 15: The maximum relative error of the median and dispersion in IM terms based on CLHS.**

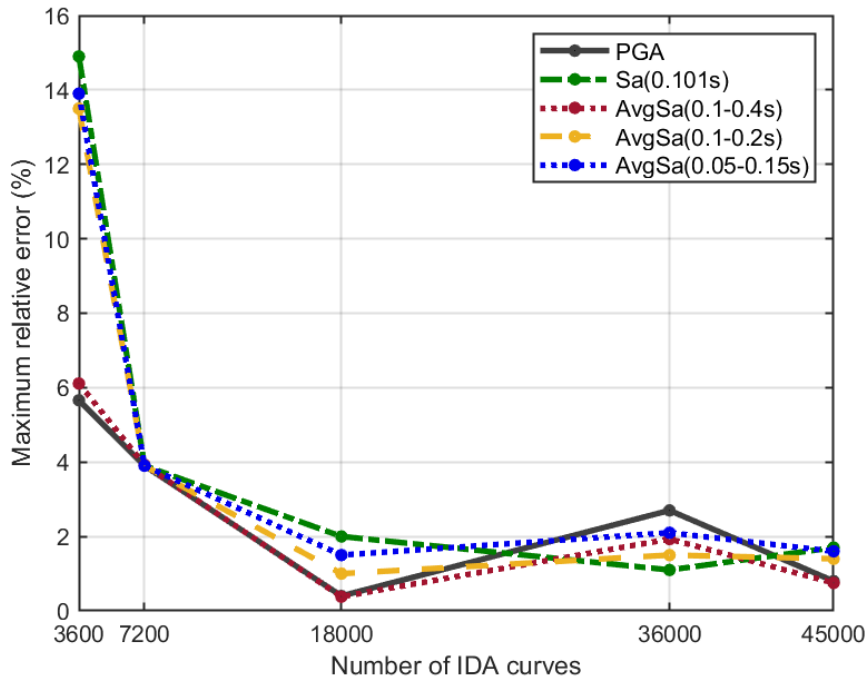


Figure 16: The maximum relative error of the median and dispersion in IM terms based on Sobol sequence.

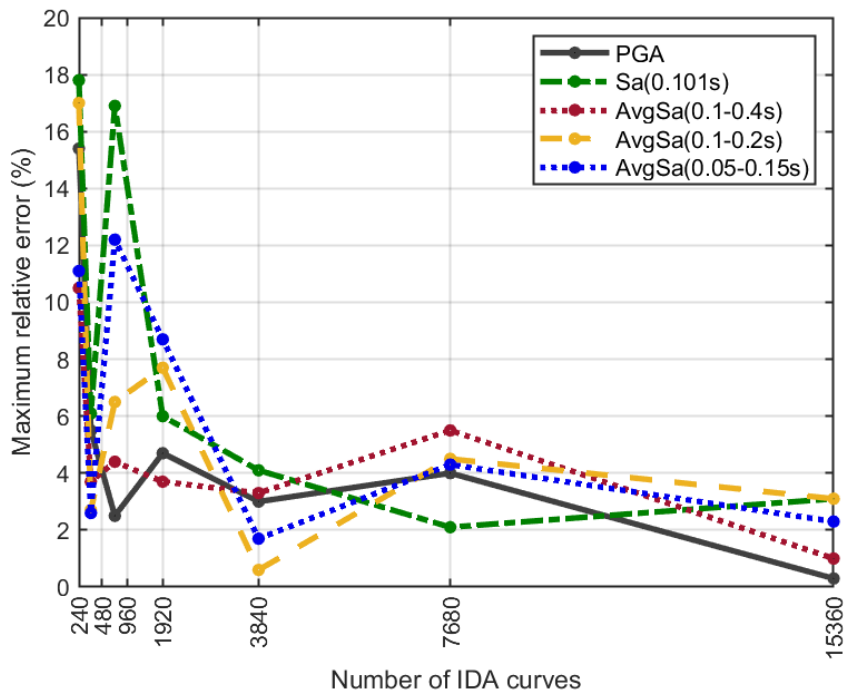


Figure 17: The maximum relative error of the median and dispersion in IM terms based on PLHS.



## 4. Conclusion

The present deliverable employed techniques, namely LHS, Sobol sequences and FOSM approach, to investigate the impact of model parameter uncertainties on the seismic performance of equipment within a nuclear power plant. Additionally, the study explored the feasibility of using progressive sample generation algorithms as an alternative to the CLHS, aiming to achieve comparable precision while reducing computational cost.

The results indicated that Monte Carlo simulation with progressive LHS and Sobol sequences indeed provide outcomes of equivalent precision compared to the traditional LHS approach. As presented even through the simplified examples, LHS is always a good option as a sampling approach, while it is observed that PLHS offers the added advantage of lower and controllable computational expenses. On the other hand, the FOSM method exhibited less accuracy, particularly concerning the examined IMs. Furthermore, the scalability of the FOSM approach becomes more challenging when dealing with numerous parameters, thus limiting its applicability.

Regarding the selection of the appropriate IM for assessing equipment component fragility curves, spectral acceleration at the fundamental period of the component displayed the least dispersion, thus demonstrating commendable overall performance. However, it should be noted that each component possesses its own unique eigenperiod, posing challenges in identifying a single "optimal" period for analysis. Alternatively, when aiming for an IM that is largely independent of individual component characteristics, utilizing the AvgSa over a range of short periods yielded near-optimal and practically period-independent results.

In summary, the findings of this study shed light on the effectiveness of Monte Carlo simulation with LHS and especially progressive LHS in analysing model parameter uncertainties. However, for rapid assessments of the first two statistical moments, FOSM analysis can be useful, especially in linear or near-linear small-size models. Yet, it tends to lose precision with increasing nonlinearity. Moreover, the selection of an appropriate IM is of utmost importance in accurately characterizing component fragility curves, and the choice between Spectral Acceleration at the fundamental period, AvgSa over short periods and the ubiquitous Peak Ground Acceleration depends on the desired balance between precision and practicality in the given context.

## 5. Acknowledgments

We would like to thank Pablo Garcia de Quevedo Iñarritu for creating the structural model of the reactor building in Opensees.

## 6. Bibliography

Adam, C., Kampenhuber, D., Ibarra L.F., & Tsantaki, S. (2017). Optimal spectral acceleration-based intensity measure for seismic collapse assessment of P-delta vulnerable frame structures. *Journal of Earthquake Engineering*, 21(7), 1189-1195.

Ancheta, T. D., Darragh, R. B., Stewart, et al. (2013). *PEER NGA-west2 database* (Vol. 172). Berkeley, CA: Pacific Earthquake Engineering Research Center.

ASCE 4-16. (2017). *Seismic Analysis of Safety-Related Nuclear Structures*. American Society of Civil Engineers. Reston, VA, USA.

ASCE 43-19. (2019). *Seismic Design Criteria for Structures, Systems, and Components in Nuclear Facilities*. American Society of Civil Engineers. Reston, VA, USA.



Bakalis, K., Kohrangi, M., Vamvatsikos, D. (2018) Seismic intensity measures for above-ground liquid storage tanks. *Earthquake Engineering & Structural Dynamics* 47(9):1844–1863. <https://doi.org/10.1002/eqe.3043>

Bakalis, K., & Vamvatsikos, D. (2018). Seismic fragility functions via nonlinear response history analysis. *Journal of structural engineering*, 144(10), 04018181.

Bojórquez, E., & Iervolino, I. (2011). Spectral shape proxies and nonlinear structural response. *Soil Dynamics and Earthquake Engineering*, 31(7), 996–1008.

Briggs, L L, & Nuclear Engineering Division. Uncertainty quantification approaches for advanced reactor analyses. United States. <https://doi.org/10.2172/956921>

Charnpis, D. C., & Panteli, P. L. (2004). A heuristic approach for the generation of multivariate random samples with specified marginal distributions and correlation matrix. *Computational statistics*, 19, 283-300.

Chen, J. T., Chokshi, N. C., Kenneally, R. M., Kelly, G. B., Beckner, W. D., McCracken, C., Murphy, A.J., Reiter, L. & Jeng, D. (1991). Procedural and submittal guidance for the individual plant examination of external events (IPEEE) for severe accident vulnerabilities (No. NUREG-1407). Nuclear Regulatory Commission, Washington, DC, USA.

Cornell, C. A., & Krawinkler, H. (2000). Progress and challenges in seismic performance assessment. *PEER Center News*, (<http://peer.berkeley.edu/news/2000spring/index.html>) (Jan. 2014).

De Biasio, M., Grange, S., Dufour, F., Allain, F., & Petre-Lazar, I. (2014). A simple and efficient intensity measure to account for nonlinear structural behavior. *Earthquake Spectra*, 30(4), 1403-1426.

Der Kiureghian, A., & Ditlevsen, O. (2009). Aleatory or epistemic? Does it matter?. *Structural Safety*, 31(2), 105-112.

Deutsch, J. L., & Deutsch, C. V. (2012). Latin hypercube sampling with multidimensional uniformity. *Journal of Statistical Planning and Inference*, 142(3), 763-772.

Dige, N., & Diwekar, U. (2018). Efficient sampling algorithm for large-scale optimization under uncertainty problems. *Computers & Chemical Engineering*, 115, 431-454.

Dolšek, M. (2009). Incremental dynamic analysis with consideration of modeling uncertainties. *Earthquake Engineering & Structural Dynamics*, 38(6), 805–825.

Dolšek, M., Fazarinc, N., Šipčić, N., García De Quevedo Iñarritu, P., Triantafyllou, G., Zentner, I., Gerontati, A. & Vamvatsikos, D. (2024). *Report title. METIS Deliverable D6.3.*

Eads, L., Miranda, E., & Lignos, D. G. (2015). Average spectral acceleration as an intensity measure for collapse risk assessment. *Earthquake Engineering and Structural Dynamics*, 44(12), 2057–2073.

Ehlers, G. (1942). The effect of soil flexibility on vibrating systems. *Beton und Eisen*, 41, 197-203. [in German].

Ellingwood, B. R., & Kinali, K. (2009). Quantifying and communicating uncertainty in seismic risk assessment. *Structural safety*, 31(2), 179-187.

EPRI (1994). Program on Technology Innovation: Methodology for developing seismic fragilities. Electric Power Research Institute, Palo Alto, CA, USA. 103959.

EPRI (2002). Program on Technology Innovation: Seismic fragility application guide. Electric Power Research Institute, Palo Alto, CA, USA. 1002988.

## D6.4 Report on efficient uncertainty quantification and propagations techniques



EPRI (2007). Program on Technology Innovation: Validation of CLASSI and SASSI Codes to Treat Seismic Wave Incoherence in Soil-Structure Interaction (SSI) Analysis of Nuclear Power Plant Structures. Electric Power Research Institute, Palo Alto, CA, USA. 1015111.

EPRI (2009). Program on Technology Innovation: Seismic fragility application update guide. Electric Power Research Institute (EPRI), Palo Alto, CA, USA.

EPRI (2018). Program on Technology Innovation: Seismic Fragility and Seismic Margin Guidance for Seismic Probabilistic Risk Assessments. Electric Power Research Institute, Palo Alto, CA, USA. 3002012994.

FEMA P-58-1 (2018). Seismic performance assessment of buildings, Volume 1 – Methodology Second Edition. Prepared for the Federal Emergency Management Agency by the Applied Technology Council. Washington, DC, USA.

Fox, B. L. (1986). ACM Algorithm 647. Implementation and relative efficiency of quasirandom sequence generators. *ACM Transactions on Mathematical Software*, 12(3), 362-376.

Goldschmidt, K., & Sadegh-Azar, H. (2021). Safety-related fundamentals of earthquake design, *Bauingenieur*, 96(12), 411-420.

Goldschmidt, K., Sadegh-Azar, H., Sevbo, O., Richard, B., Garcia, P., Bazzurro, P., & Vamvatsikos, D. (2022). Innovative approaches for seismic fragility analysis within METIS project. SMiRT 26th International Conference on Structural Mechanics in Reactor Technology, Berlin/Potsdam, Germany.

Hadjian, A. H., Smith, C. B., Haldar, & A., Ibanez, P. (1977). Variability in engineering aspects of structural modeling. Proceedings, 6th World Conference on Earthquake Engineering, New Delhi, India.

Halton, J. H. (1960). On the efficiency of certain quasi-random sequences of points in evaluating multi-dimensional integrals. *Numerische Mathematik*, 2, 84-90.

Haviland, R. (1976). A study of the uncertainties in the fundamental translational periods and damping values for real buildings. Massachusetts Institute of Technology, Boston, MA, USA.

Helton, J. C., & Davis, F. J. (2003). Latin hypercube sampling and the propagation of uncertainty in analyses of complex systems. *Reliability Engineering & System Safety*, 81(1), 23-69.

Hou, T., Nuyens, D., Roels, S., & Janssen, H. (2019). Quasi-Monte Carlo based uncertainty analysis: Sampling efficiency and error estimation in engineering applications. *Reliability Engineering & System Safety*, 191, 106549.

Huang, Y. N., Whittaker, A. S., & Luco, N. (2011). A probabilistic seismic risk assessment procedure for nuclear power plants:(I) Methodology. *Nuclear Engineering and Design*, 241(9), 3996-4003.

Iman, R. L., & Conover, W. J. (1980). Small sample sensitivity analysis techniques for computer models. with an application to risk assessment. *Communications in statistics-theory and methods*, 9(17), 1749-1842.

Jayaram, N., Lin, T., & Baker, J. W. (2011). A computationally efficient ground-motion selection algorithm for matching a target response spectrum mean and variance. *Earthquake Spectra*, 27(3), 797-815.

Kazantzi, A. K., & Vamvatsikos, D. (2015). Intensity measure selection for vulnerability studies of building classes. *Earthquake Engineering and Structural Dynamics*, 44(15), 2677-2694.

Kennedy, R. P., Cornell, C. A., Campbell, R. D., Kaplan, S., & Perla, H. F. (1980). Probabilistic seismic safety study of an existing nuclear power plant. *Nuclear Engineering and Design*, 59(2), 315-338.



- Kim, C., Cha, E.J., & Shin, M. (2022). Seismic performance assessment of NPP concrete containments considering recent ground motions in South Korea. *Nuclear Engineering and Technology*, 54(1), 386-400.
- Kohrangi, M., Bazzurro, P., & Vamvatsikos, D. (2016). Vector and scalar IMs in structural response estimation, Part I: Hazard Analysis. *Earthquake Spectra*, 32(3), 1507–1524.
- Kohrangi, M., Bazzurro, P., Vamvatsikos, D., & Spillatura, A. (2017). Conditional spectrum-based ground motion record selection using average spectral acceleration. *Earthquake Engineering & Structural Dynamics*, 46(10), 1667-1685.
- Kranz, S., Strohm, A., Gocht, T., Sadegh-Azar, H., & Schubert, T. (2015). Seismic robustness of a filtered containment venting system. SMiRT 23rd International Conference on Structural Mechanics in Reactor Technology, Manchester, UK.
- Lamprey, J. A., & Boore, D.M. (2007). Beyond  $S_{aGMrotI}$ : Conversion to  $S_{aArb}$ ,  $S_{aSN}$ , and  $S_{aMaxRot}$ . *Bulletin of the Seismological Society of America*, 97(5), 1511-1524.
- Lee, T. H., & Mosalam, K. M. (2005). Seismic demand sensitivity of reinforced concrete shear-wall building using FOSM method. *Earthquake engineering & structural dynamics*, 34(14), 1719-1736.
- Liel, A. B., Haselton, C. B., Deierlein, G. G., & Baker, J. W. (2009). Incorporating modeling uncertainties in the assessment of seismic collapse risk of buildings. *Structural safety*, 31(2), 197-211.
- Marseguerra, M., & Zio, E. (2004). Monte Carlo estimation of the differential importance measure: application to the protection system of a nuclear reactor. *Reliability Engineering & System Safety*, 86(1), 11-24.
- MathWorks. (2023). MATLAB [Software]. The MathWorks, Inc. <https://www.mathworks.com>
- McKay, M.D., Conover, W. J., & Beckman, R. (1979). A comparison of three methods for selecting values of input variables in the analysis of output from a computer code. *Technometrics*, 21(2), 239–245.
- Melchers, R. (2002). Structural reliability analysis and prediction. Wiley: New York.
- Metropolis, N., & Ulam, S. (1949). The Monte Carlo Method. *Journal of the American Statistical Association*, 44(247), 335-341.
- Moehle, J., & Deierlein, G. G. (2004). A framework methodology for performance-based earthquake engineering. *13th World Conference on Earthquake Engineering*, Vancouver, Canada.
- Noh, Y., Chang, K., Seo, Y., & Chang, D. (2014). Risk-based determination of design pressure of LNG fuel storage tanks based on dynamic process simulation combined with Monte Carlo method. *Reliability Engineering & System Safety*, 129, 76-82.
- OpenSees (2006). Open System for Earthquake Engineering Simulation, Pacific Earthquake Engineering Research Center, University of California, Berkeley, URL: <http://opensees.berkeley.edu/>
- Owen, A.B. (1992). Orthogonal arrays for computer experiments, integration and visualization. *Statistica Sinica*. 2, 439–452.
- Pinto, P., Giannini, R., & Franchin, P. (2004). Seismic reliability analysis of structures. IUSS Press: Pavia, Italy.
- Python Software Foundation. (2021). Python Language Reference, version 3.9. Retrieved from <http://www.python.org>
- Sadegh-Azar, H., & Hasenbank-Kriegbaum, T.D. (2014). Probabilistic Seismic Analysis of Existing Industrial Facilities. In: Klinkel, S., Butenweg, C., Lin, G., Holtschoppen, B. (eds) Seismic Design of Industrial Facilities. Springer Vieweg, Wiesbaden. DOI: 10.1007/978-3-658-02810-7\_9



- Sallaberry, C. J., Helton, J. C., & Hora, S. C. (2008). Extension of Latin hypercube samples with correlated variables. *Reliability Engineering & System Safety*, 93(7), 1047-1059.
- Syed, S., & Gupta, A. (2015). Seismic fragility of RC shear walls in nuclear power plant part 1: characterization of uncertainty in concrete constitutive model. *Nuclear Engineering and Design*, 295, 576-586.
- Sobol, I. M. (1967). On the distribution of points in a cube and the approximate evaluation of integrals. *USSR Computational Mathematics and Mathematical Physics*, 7(4), 784-802.
- Sobol, I. M. (1976). Uniformly distributed sequences with an additional uniform property. *USSR Computational Mathematics and Mathematical Physics*, 16(5), 236-242.
- Sobol, I. M. (1979). On the systematic search in a hypercube. *SIAM Journal on Numerical Analysis*, 16(5), 790-793.
- Tang, B. (1993). Orthogonal array-based Latin hypercubes. *Journal of the American statistical association*, 88(424), 1392-1397.
- Tong, C. (2006). Refinement strategies for stratified sampling methods. *Reliability Engineering & System Safety*, 91(10-11), 1257-1265.
- Van der Corput, J.G. (1935). Verteilungsfunktionen, Proceedings of the Koninklijke Akademie van Wetenschappen te Amsterdam (in German), 38, 813-821.
- Vamvatsikos, D., & Cornell, C. A. (2002). Incremental dynamic analysis. *Earthquake Engineering & Structural Dynamics*, 31(3), 491-514.
- Vamvatsikos, D., & Cornell, C. A. (2005). Developing efficient scalar and vector intensity measures for IDA capacity estimation by incorporating elastic spectral shape information. *Earthquake engineering & structural dynamics*, 34(13), 1573-1600.
- Vamvatsikos, D., & Fragiadakis, M. (2010). Incremental dynamic analysis for estimating seismic performance sensitivity and uncertainty. *Earthquake engineering & structural dynamics*, 39(2), 141-163.
- Vamvatsikos, D. (2014). Seismic performance uncertainty estimation via IDA with progressive accelerogram-wise Latin hypercube sampling. *ASCE Journal of Structural Engineering*, 140(8), A4014015.
- Vestrucci, P., Santucci, R., & Calderan, R. (1991). Monte Carlo simulation of crew responses to accident sequences. *Reliability Engineering & System Safety*, 31(2), 129-144.
- Wang, W., Cammi, A., Di Maio, F., Lorenzi, S., & Zio, E. (2018). A Monte Carlo-based exploration framework for identifying components vulnerable to cyber threats in nuclear power plants. *Reliability Engineering & System Safety*, 175, 24-37.
- Wikipedia contributors (2024). Latin hypercube sampling. In *Wikipedia*. URL: [https://en.wikipedia.org/wiki/Latin\\_hypercube\\_sampling](https://en.wikipedia.org/wiki/Latin_hypercube_sampling)
- Willaume, P., & Noret, E. (2011). Présentation du modèle brochette (Report No. DT-PMPE-00234-002-B). [Confidential]. EDF.
- Wolf, J.P. (1998). Simple physical models for foundation dynamics. *Developments in Geotechnical Engineering*, 83, 1-70.
- Yang, T. Y., Moehle, J., Stojadinovic, B., & Der Kiureghian, A. (2009). Seismic performance evaluation of facilities: Methodology and implementation. *Journal of Structural Engineering*, 135(10), 1146-1154.
- Ye, K. Q. (1998). Orthogonal column Latin hypercubes and their application in computer experiments. *Journal of the American Statistical Association*, 93(444), 1430-1439.

## D6.4 Report on efficient uncertainty quantification and propagations techniques



Zentner, I., Gündel, M., & Bonfils, N. (2017). Fragility analysis methods: Review of existing approaches and application. *Nuclear Engineering and Design*, 323, 245-258.

Zentner, I., Humbert, N., Ravet, S., & Viallet, E. (2011). Numerical methods for seismic fragility analysis of structures and components in the nuclear industry - Application to a reactor coolant system. *Georisk*, 5(2), 99-109.